Interpreting an apoptotic corpse as anti-inflammatory involves a chloride sensing pathway

Interpreting an apoptotic corpse as anti-inflammatory involves a chloride sensing pathway

Justin S. A. Perry[1,2,10*], Sho Morioka[1,2,11*], Christopher B. Medina[1,2], J. Iker Etchegaray[1,2], Brady Barron[1,3], Michael H. Raymond[1,4], Christopher D. Lucas[1,2,7], Suna Onengut-Gumuscu[5,6], Eric Delpire[8], and Kodi S. Ravichandran[1,2,9,^].

[1]The Center for Cell Clearance,
[2]Department of Microbiology, Immunology, and Cancer Biology,
[3]Pharmacology Graduate Program,
[4]Neuroscience Graduate Program,
[5]Department of Medicine, Division of Endocrinology and Metabolism,
[6]Center for Public Health Genomics, University of Virginia, Charlottesville, Virginia, USA.
[7]Centre for Inflammation Research, University of Edinburgh, Edinburgh, Scotland, UK.
[8]Department of Anesthesiology, Vanderbilt University School of Medicine, Nashville, TN, USA.
[9]Inflammation Research Centre, VIB, and the Department of Biomedical Molecular Biology, Ghent University, Ghent, Belgium.
[10]Immunology Program, Sloan Kettering Institute, Memorial Sloan Kettering Cancer Center, New York, NY, USA
[11]Department of Medicine, Division of Nephrology and CIIR, University of Virginia Health System, Charlottesville, VA, USA

*These authors contributed equally to this work.

^Corresponding author: Ravi@virginia.edu

ABSTRACT

Apoptotic cell clearance (efferocytosis) elicits an anti-inflammatory response by phagocytes, but the mechanisms underlying this response are still being defined. While deciphering gene programs induced in phagocytes after corpse-ingestion, we uncovered a chloride-sensing signaling pathway that controls both the phagocyte appetite and its anti-inflammatory response. First, within engulfing phagocytes, the solute carrier 12 (SLC12) family members SLC12A2 and SLC12A4 are actively modulated. Interfering with SLC12A2 expression or function led to significantly enhanced corpse uptake per phagocyte, while loss of SLC12A4 inhibited corpse uptake. In SLC12A2-deficient phagocytes the canonical anti-inflammatory program was replaced by pro-inflammatory and oxidative stress-associated gene programs. The kinases WNK1-OSR1-SPAK that function upstream of SLC12A2 also similarly affected efferocytosis via chloride entry/exit across the plasma membrane of phagocytes. The 'switch' to pro-inflammatory sensing of apoptotic cells was due to disruption of the chloride-sensing pathway and not corpse overload or poor degradation, and this pro-inflammatory switch was reversed by a chloride ionophore. Collectively, the WNK1-OSR1-SPAK-SLC12A2/SLC12A4 chloride-sensing pathway and chloride flux in phagocytes act as key modifiers of how a phagocyte interprets the engulfed apoptotic corpse.

Every day, we turnover >200 billion cells in the body via apoptosis as part of normal homeostasis[1-4]. These apoptotic cells are removed by the process of 'efferocytosis', which involves specific recognition and uptake by professional phagocytes (such as macrophages and dendritic cells) and non-professional phagocytes (such as epithelial cells)[5-9]. Research from a number of laboratories has identified a series of steps in efferocytosis, including: the release of soluble factors from apoptotic cells ('find-me' signals or the 'smell' phase) that help the phagocyte sense the corpses, the specific ligands on the apoptotic cell surface ('eat-me' signals) that are recognized by specific receptors on the phagocytes (the 'taste' phase), and corpse internalization involving extensive cytoskeletal reorganization and subsequent digestion of corpse contents (the 'ingestion' phase)[10-15].

It is now well-established that defects or failures in proper removal of apoptotic cells can result in inflammation with a predilection toward autoimmune disease, including systemic lupus erythematosus and chronic inflammation-associated diseases, such as atherosclerosis and ulcerative colitis[1, 3, 16, 17]. Thus, understanding the key molecules and mechanisms that regulate the distinct steps of efferocytosis can help target these players and pathways, and potentially modulate efferocytosis and inflammation. Ingesting a corpse with potentially 'dangerous' contents and managing this cargo while maintaining homeostasis is a unique challenge for the phagocyte. An added complexity is that most tissues have fewer phagocytes than the number of cells undergoing apoptosis, requiring individual phagocytes to successively ingest multiple apoptotic targets[1, 2, 4]. While significant progress has been made in deciphering key membrane receptors on phagocytes and ligands on apoptotic cells, our knowledge of molecular players regulating the phagocyte response *after* a corpse is ingested is just emerging. Efferocytic phagocytes also perform two concurrent actions: dampen pro-inflammatory mediators and activate production of anti-inflammatory mediators (i.e. 'immunosuppressive')[1]. Thus, defining molecular players that regulate phagocyte responses after corpse uptake and from becoming pro-inflammatory are important, and a focus of this work.

While some genes in phagocytes are induced by specific find-me signals[18], others can be initiated only by phagocyte:apoptotic cell contact (without corpse internalization)[19-22]. However, our knowledge of specific transcriptional programs initiated after a corpse is internalized is limited. To address this, we performed RNAseq analysis, comparing RNA from phagocytes either eating apoptotic cells normally, or phagocytes capable of binding but not internalizing corpses (**Fig. 1a**).

Also, to better distinguish the phagocyte-derived RNA (from that of the corpse), we used hamster LR73 fibroblasts as phagocytes and apoptotic human Jurkat T cells as targets. We utilized LR73 fibroblasts to overcome the issue of corpse-derived RNA contamination in the phagocyte RNAseq datasets [23]; comparison of hamster versus human coding genomes allowed us to specifically focus on phagocyte-specific gene modulation (which was not feasible with mouse versus human comparison). In subsequent analyses, we addressed gene programs induced after corpse internalization from those induced by corpse contact/soluble factors (**Fig. 1a**). About 5x more genes were modulated in phagocytes by corpse internalization compared to apoptotic cell supernatant/contact (**Fig. 1a**). Among the *corpse internalization-specific* genes, phagocytes upregulated gene programs linked to chloride transport/cell volume, carbohydrate metabolism, anti-apoptotic responses, cell adhesion/motility, actin/cytoskeleton rearrangement, and anti-inflammatory responses (**Fig. 1b**), while downregulating genes associated with fatty acid oxidation, oxidative phosphorylation, pro-apoptotic responses, cholesterol metabolism, oxidative stress, and pro-inflammatory responses (**Fig. 1b**). Thus, upon engulfing an apoptotic corpse, phagocytes induce distinct gene programs.

For further in-depth analysis, we picked SLC12 (*sol*ute *c*arrier family 12) pathway genes that were part of the cell volume/cell shape gene program for several reasons. First, modulation of a number of SLC family members during efferocytosis was recently noted[15], although the function of SLC12 family is not defined. Second, within the SLC12 family, multiple genes were coordinately regulated (**Supplementary Table 1**), including the transporter *Slc12a2* (encoding SLC12A2, also called NKCC1), *Slc12a4* (encoding SLC12A4, also called KCC1), and the upstream kinases that regulate SLC12A2 and SLC12A4, namely *Oxsr1* (encoding OSR1) and *Stk39* (encoding SPAK**)**. Third, SLC12A2 and SLC12A4 are linked to chloride flux into and out of cells, in particular in the kidney[24], and little is known about the potential role of chloride flux during efferocytosis. After confirming the transcriptional changes noted in the RNAseq within the SLC12 pathway genes in phagocytes by qPCR (**Extended Data Fig. 1a**), we addressed the functional relevance of this pathway and made several striking observations.

Surprisingly, targeted deletion of *Slc12a2* via CRISPR/Cas9 or siRNA-mediated knockdown in LR73 phagocytes resulted in significantly *enhanced* uptake of apoptotic corpses (**Fig. 2a and Extended Data Fig. 1b,c**). Further, treatment of phagocytes with bumetanide, an

inhibitor of SLC12A2 transporter activity, also led to increased corpse uptake (**Extended Data Fig. 1d,e**); bumetanide did not further increase efferocytosis in phagocytes in *Slc12a2*-deficient phagocytes (**Extended Data Fig. 1f**). This greater uptake was dependent on recognition of PtdSer exposed on apoptotic cells (**Extended Data Fig. 1g**) and was seen in *Slc12a2*-deficient LR73 phagocytes over an extended period of co-culture with apoptotic cells (**Fig. 2a**).

We next tested SLC12A2 function in professional phagocytes such as macrophages via multiple approaches. First, we performed genetic deletion of *Slc12a2* ex vivo via CRISPR/Cas9 in ER-Hoxb8[25] immortalized primary bone marrow-derived macrophages, and the loss of SLC12A2 significantly increased efferocytosis (**Fig. 2b and Extended Data Fig. 1h**). Second, loss-of-function mutations in SLC12 family protein members (including SLC12A2) result in an array of human diseases[24, 26, 27], and incorporating a 11-bp deletion in exon 22 observed in a human patient into the mouse *Slc12a2* gene locus (*Slc12a2*^{mut}) results in multiple phenotypes[28-30] and early lethality in homozygous mice. Using bone marrow from this mouse strain[29], we derived macrophages (BMDMs) that displayed similarly increased efferocytosis (**Fig. 2c**). Third, treatment of wild type BMDMs (**Fig. 2d**) or peritoneal macrophages (pMacs; **Extended Data Fig. 1e**) *in vitro* with the SLC12A2 inhibitor bumetanide also enhanced efferocytosis. Fourth, using two different *in vivo* models, we assessed whether disruption of SLC12A2 function would lead to increased efferocytosis. Thymic macrophage engulfment of apoptotic thymocytes induced by dexamethasone after bone marrow transplantation (see experimental model; **Fig. 2e**), and apoptotic cell uptake by peritoneal macrophages (**Extended Data Fig. 1i**) were both enhanced after inhibition of SLC12A2. Imaging flow cytometry (*ImageStreamX*) of *Slc12a2*-deficient LR73 phagocytes showed more corpse uptake on a per cell basis (**Fig. 2f**); whereas control phagocytes mostly engulfed 1 to 2 corpses under these assay conditions, ~45% of efferocytic *Slc12a2*-deficient phagocytes contained 4 or more corpses (**Fig. 2f**). Similarly, fluorescent microscopy of *Slc12a2*-deficient macrophages revealed significantly increased efferocytosis on a per-cell basis (**Extended Data Fig. 1j**). Collectively, these data suggest that SLC12A2 acts as a natural brake on apoptotic cell uptake, and that interfering with SLC12A2 function leads to increased efferocytosis by both professional and non-professional phagocytes.

The enhanced corpse-derived fluorescence seen with *Slc12a2*-deficient phagocytes was not due to defective corpse degradation based on several criteria. First, we fed apoptotic cells labeled

with TAMRA, a dye that directly labels peptides and proteins in apoptotic cells, and monitored degradation of TAMRA signal via flow cytometry in both LR73 phagocytes and macrophages (**Fig. 3a-c**). Although rates of degradation varied between LR73 phagocytes and macrophages (i.e. non-professional vs. professional phagocytes), when paired control and *Slc12a2*-deficient phagocytes are compared (**Fig. 3a-c**), the loss of SLC12A2 did not affect the rates of corpse degradation. Second, by time lapse microscopy, we observed similar kinetics of corpse degradation between control and *Slc12a2*-deficient phagocytes (**Supplementary Videos 1-6**). There was no significant difference in lysosomal pH in efferocytic phagocytes between control and *Slc12a2*-deficient LR73 phagocytes or macrophages (**Fig. 3d, e**), and inhibition of lysosomal acidification did not alter the *Slc12a2*-deficient LR73 phagocyte or macrophage phenotype of enhanced apoptotic cell uptake (**Fig. 3f, g**). Finally, labeling apoptotic cells with the reagent DQ-Red-BSA, whose cleavage by cathepsin protease activity within the acidic phagolysosome induces the DQ-Red fluorescence, revealed comparable phagolysosomal activity in the control and SLC12A2-deficient LR73 cells and macrophages; we also noted increased total signal in *Slc12a2*-deficient phagocytes relative to control phagocytes (**Fig. 3h, i**). Thus, our data suggest that SLC12A2 dampens phagocyte uptake on a per cell basis, without an apparent effect on lysosomal acidification or corpse degradation.

Interestingly, another SLC12 family member, SLC12A4, acts in opposition to SLC12A2 during regulatory volume change [31]. Although *Slc12a4* was only modestly downmodulated transcriptionally and by total protein after corpse internalization (**Extended Data Fig. 1a and 2a**), targeting of *Slc12a4* by CRISPR/Cas9-mediated deletion or siRNA-mediated silencing in LR73 phagocytes led to a reduction in apoptotic cell uptake (**Extended Data Fig. 2b-e**). This reduced uptake was not a delay in eating, as this was seen even after 8-hour co-culture with apoptotic cells (**Extended Data Fig. 2c, e**). Thus, SLC12A2 and SLC12A4 may functionally counterbalance each other during efferocytosis. Interestingly, when we performed double targeting of *Slc12a2* and *Slc12a4* by siRNA-mediated knockdown of *Slc12a4* in the context of *Slc12a2*-deficient LR73 cells, double-deficient phagocytes still showed greater efferocytosis (**Extended Data Fig. 2f**), suggesting that SLC12A2 deficiency is a dominant phenotype over the loss of SLC12A4.

To address the consequence of Slc12a2 deficiency in efferocytic phagocytes, we performed RNAseq analysis of efferocytic control and *Slc12a2*-deficient phagocytes (**Fig. 4a,b**). Normally,

efferocytosis elicits multiple distinct transcriptional programs in engulfing phagocytes (**Fig. 1b**). Strikingly, *Slc12a2*-deficient phagocytes showed unexpected changes in several of these signatures, including reversals of the anti-inflammatory and oxidative stress signatures, as well as a strong increase in a pro-inflammatory gene program (**Fig. 4b**), suggesting that loss of SLC12A2 affects how a phagocyte normally interprets apoptotic cell uptake as anti-inflammatory. Interestingly, many of the anti-inflammatory and pro-inflammatory genes found to be dysregulated in engulfing *Slc12a2*-deficient phagocytes have genetic /functional linkages with chronic inflammatory, auto-inflammatory, and autoimmune diseases (**Supplementary Table 2**).

When we re-introduced *Slc12a2* cDNA into *Slc12a2*-deficient efferocytic phagocytes, this reversed the greater corpse uptake and pro-inflammatory gene induction, confirming that the observed pro-inflammatory signature was in fact due to the absence of SLC12A2 (**Extended Data Fig. 3a,b**). The pro-inflammatory signature noted above could be a general property of phagocytes over-eating more corpses. To address this, we used LR73 phagocytes overexpressing the PtdSer receptor TIM-4, which increases uptake on a per cell basis [32-35]. We then sorted engulfing (i.e. CypHer5E+) phagocytes from three conditions: control phagocytes with normal uptake, TIM4 overexpressing phagocytes with increased uptake, and phagocytes lacking SLC12A2 that also have enhanced uptake. Despite eating more corpses, the TIM4-overexpressing phagocytes did not show upregulation of pro-inflammatory signature genes, contrasting with *Slc12a2*-deficient phagocytes (**Fig. 4c**). Further, siRNA-mediated knockdown of *Slc12a2* in TIM4 overexpressing cells induced upregulation of many of the pro-inflammatory signature genes (**Extended Data Fig. 3c**). This latter phenotype was less pronounced than *Slc12a2*-deficient phagocytes, likely because TIM4 is stably overexpressed and siRNA knockdown efficiency can vary between cells in a population. Thus, the pro-inflammatory gene signature of *Slc12a2*-deficient efferocytic phagocytes is not simply a corpse-overload effect, and that loss of *Slc12a2* alters the anti-inflammatory response during efferocytosis.

Both SLC12A2 and SLC12A4 are regulated by upstream kinases, as part of a pathway for chloride sensing and chloride flux in cells. When there is chloride efflux from a cell, it is sensed by one of the four members of the '*With-No-lysine Kinase*' (WNK) family of Ser/Thr kinases (**Fig. 5a**)[24]. WNK1, a broadly and ubiquitously expressed member, becomes activated by chloride efflux and subsequently phosphorylates the downstream serine/threonine kinases OSR1 and SPAK

(encoded by the genes *Oxsr1* and *Stk39*, respectively**; Fig. 5a**)[36-41]. In our RNAseq, we noted that both *Oxsr1* and *Stk39* are transcriptionally upregulated in phagocytes after corpse internalization (**Fig. 1c).** OSR1 and SPAK, in turn, phosphorylate both SLC12A4 and SLC12A2 leading to decreased SLC12A4-mediated chloride efflux and increased SLC12A2-mediated chloride influx (**Fig. 5a**)[31, 39]. Although phosphorylation on multi-pass transmembrane proteins are difficult to detect, we could observe increased phosphorylation on both SLC12A2 and SLC12A4 proteins in a time course of efferocytosis (**Extended Data Fig. 4a**). Therefore, we next addressed the functional relevance of OSR1, SPAK, and WNK1. Knockdown of either OSR1 or SPAK resulted in greater apoptotic cell uptake both at early and late time points (**Fig. 5b,c and Extended Data Fig. 4b,c**). Furthermore, deletion/reduction of *Wnk1* expression either via CRISPR/Cas9 deletion or siRNA-mediated knockdown in LR73 phagocytes resulted in significantly greater corpse uptake, essentially phenocopying *Slc12a2* deficiency (**Fig. 5d,e and Extended Data Fig. 4d-f**).

We then assessed whether WNK proteins regulate rate of apoptotic cell engulfment *in vivo*. After confirming that BMDMs or peritoneal macrophages treated with a pan-WNK inhibitor WNK463 [42] *in vitro* enhanced efferocytosis (**Fig. 5f,g**), we injected WNK463 into the peritoneum of mice prior to dexamethasone injection (thymic engulfment model; **Fig. 5h**) or injection of apoptotic Jurkat cells (peritoneal engulfment model; **Fig. 5i**); in both cases we saw increased apoptotic cell uptake by resident macrophages *in vivo*. Thus, the WNK1–SLC12A2 chloride sensing pathway acts as a brake *in vitro* and *in vivo* to control the 'appetite' of phagocytes for apoptotic cells.

As chloride is important for many biological functions [43-45], we hypothesized that chloride flux may also affect different aspects of efferocytosis. As chloride flux is well-linked to cell volume regulation, we initially tested the possible impact of chloride on phagocyte cell size during efferocytosis. We analyzed the forward scatter area (FSC-A) of engulfing phagocytes by flow cytometry, a commonly used indicator of cell size change, which allowed us to gate specifically on engulfing phagocytes and assess FSC-A changes in thousands of phagocytes. Interestingly, control phagocytes eating corpses routinely had a modest but detectable *decrease* in cell size, suggesting that despite engulfing another cell, the phagocyte volume is actively controlled. While *Slc12a2*-deficient LR73 cells were slightly smaller in size basally, engulfing *Slc12a2*-deficient phagocytes became 40% larger compared to controls (**Extended Data Fig. 5a**). This was not

unique to LR73 phagocytes, as BMDMs from *Slc12a2*^{mut} mice and *Slc12a2*-deficient BMDMs were also slightly smaller in size basally, but became larger during efferocytosis (**Extended Data Fig. 5b,c**). Similarly, engulfing *Wnk1*-deficient phagocytes were also larger than control *Wnk1*-sufficient phagocytes (**Extended Data Fig. 5d**). Importantly, the larger size of *Slc12a2*- or *Wnk1*-deficient phagocytes does not appear to be due to 'over-eating' *per se*, as LR73 phagocytes overexpressing the PtdSer receptor TIM4 do ingest more corpses, yet do not show larger cell size (**Extended Data Fig. 5e,f**). When we compared *Slc12a2* and *Slc12a4* deficient phagocytes, *Slc12a4*-deficient cells were modestly larger in size prior to addition of apoptotic corpses, and although efferocytosis was attenuated by loss of *Slc12a4*, these *Slc12a4*-deficient phagocytes that did engulf apoptotic cells were smaller than control phagocytes (**Extended Data Fig. 5g**). Thus, the SLC12 members and upstream regulatory kinases can influence phagocyte cell size during efferocytosis.

We next tested if enhanced engulfment in *Slc12a2*-deficient phagocytes required chloride flux across the plasma membrane. We treated phagocytes with a chloride ionophore tributyltin chloride (TBTC), which forces extracellular chloride into the phagocyte cytosol. Treatment with TBTC reversed the increased uptake and larger FSC-A/ cell size phenotype after corpse uptake observed in *Slc12a2*-deficient phagocytes (**Fig. 6a and Extended Data Fig. 5h**). To directly assess chloride flux during efferocytosis, we used the cell permeable chloride-sensitive fluorescent dye MQAE [46, 47]. MQAE reversibly binds chloride in the cytosol, with the fluorescence signal for MQAE being quenched (i.e. decreased), at higher cytosolic chloride concentrations (**Fig. 6b**)[46, 47]. Further, MQAE fluorescence is not affected by pH or bicarbonate[47], allowing its use during phagocytosis assays. We first confirmed that phagocytes can be labeled with MQAE and the baseline MQAE fluorescence was quenched with forced entry of chloride through TBTC (**Extended Data Fig. 6a**). During efferocytosis, phagocytes maximally engulfing CypHer5E-labeled apoptotic targets (CypHer5E 'bright') showed less intracellular chloride that is revealed as MQAE^{high} fluorescence in the flow cytometry readout (**Fig. 6b,c and Extended Data Fig. 6b**). These data suggest that the efflux of cytosolic chloride from the engulfing phagocytes is a component of normal efferocytosis.

Next, we hypothesized that in engulfing phagocytes, the loss of SLC12A2 would result in less cytosolic chloride, while loss of SLC12A4 would result in more cytosolic chloride. siRNA

mediated knockdown of *Slc12a2* resulted in significantly more engulfing phagocytes with significantly lower cytosolic chloride level (**Fig. 6d,** quantification in **Fig. 6e and Extended Data Fig. 6c**). In contrast, TIM4 overexpressing phagocytes that also take up more corpses had similar numbers of efferocytic phagocytes with lower MQAE levels (**Extended Data Fig. 6d**). A similar reduced chloride level (i.e. more $MQAE^{high}$ cells) was also seen in *Slc12a2*^{mut} bone marrow-derived macrophages actively eating apoptotic cells (**Extended Data Fig. 6ef**). In contrast, targeting *Slc12a4* via siRNA resulted in fewer engulfing phagocytes with $MQAE^{high}$ phenotype (**Fig. 6d,e and Extended Data Fig. 6c**). We then assessed chloride flux in efferocytic phagocytes where the upstream kinases (WNK1/OSR1/SPAK) in the chloride-sensing pathway were knocked down. siRNA targeting of *Wnk1*, *Oxsr1*, or *Stk39* phenocopied the *Slc12a2*-deficient phenotype, displaying many more engulfing phagocytes with a $MQAE^{high}$ / low cytosolic chloride profile (**Extended Data Fig. 6g,** quantification in **Fig. S6g, and Extended Data Fig. 6i)**. Disruption of any one of the upstream kinases manifested similar results to the loss of SLC12A2-mediated chloride influx, further correlating with the observation seen in **Extended Data Fig. 4a**. These data suggest that components of the chloride-sensing pathway including SLC12A2, SLC12A4, and the kinases WNK1, OSR1, and SPAK contribute to chloride flux into and out of phagocytes during efferocytosis, with chloride influx acting as a 'brake' on corpse uptake.

In addressing a possible mechanism for increased uptake, we found that *Slc12a2*-deficient phagocytes bound more corpses compared to control (**Fig. 6f**). Increased binding of corpses by *Slc12a2*-deficient LR73 phagocytes was indicated by both percentage of phagocytes that bound corpses and the number of targets bound to phagocytes via MFI. Interestingly, addition of the chloride ionophore TBTC, followed by the binding assay, showed reversal of the increased corpse binding to *Slc12a2*-deficient phagocytes (**Fig. 6f**). While performing these binding experiments, we noted that a 6 h TBTC treatment was more effective in seeing significant reversal of binding in *Slc12a2*-deficient phagocytes. This prompted us to go back to the RNAseq data and re-analyze expression of genes coding for engulfment receptors in the *Slc12a2*-deficient phagocytes. In *Slc12a2*-deficient LR73 phagocytes, there was an increase in gene expression for integrin α_v and integrin β_5 that have been linked to efferocytosis, as well as molecules linked to integrin dependent signaling such as p130Cas (BCAR1), and the small GTPase RhoG and CrkI linked genetically and biochemically to efferocytosis via $\alpha_v\beta_5$ integrin (**Fig. 6g**) [48-53]. When we tested whether integrin-

dependent interaction might contribute to the increased efferocytosis observed with *Slc12a2*-deficient phagocytes, an RGDS peptide added prior to addition of apoptotic targets partially inhibited the increased corpse binding to *Slc12a2*-deficient phagocytes (almost similar to the positive control for blocking with annexin V) (**Fig. 6h**). Collectively, these data support a mechanism that the altered chloride efflux in the *Slc12a2*-deficient phagocytes leads to enhanced apoptotic cell uptake, in part, via increased expression of integrins and greater binding of apoptotic targets. While this increased integrin expression is clearly one mechanism, there could also be other modalities that remain to be explored.

To test the *in vivo* linkage between this chloride-sensing pathway and the interpretation of apoptotic cells as anti- vs. pro-inflammatory, we used a well-established apoptotic cell clearance model of low-dose LPS-induced acute lung inflammation[54]. In this model (schematic in **Fig. 7**), low-dose LPS is administered intranasally, eliciting neutrophil and monocyte infiltration, with induction of pro-inflammatory cytokines including TNFα, IL-6, and IL-1. After 24 h, neutrophils undergo apoptosis and are engulfed by lung macrophages, leading to resolution of the inflammatory response[54]. At 24 h post LPS inoculation, after the initial onset of the LPS-induced response, we intraperitoneally administered either the SLC12A2 inhibitor bumetanide or the pan-WNK kinase inhibitor WNK463. After an additional 12 h, bronchoalveolar fluid (BALF) was assessed for the resolution of the inflammatory response. Strikingly, mice treated with the SLC12A2 inhibitor bumetanide had significant levels of the pro-inflammatory cytokines IL-1α, IL-1β, IL-6, and TNFα, which were absent in vehicle control-treated mice (**Fig. 7a**). Additionally, bumetanide treated mice failed to upregulate the pro-resolution cytokine IL-10 (**Fig. 7a**). The pan-WNK inhibitor WNK463 had a similar effect, albeit less pronounced, on inflammation resolution (**Fig. 7a**). We also isolated Siglec F^+ alveolar macrophages from the same mice, and detected upregulation of the pro-inflammatory gene signature in macrophages treated with either bumetanide or WNK463 (**Fig. 7b**). The increased inflammatory cytokine production in the BALF correlated with efferocytic thymic macrophages treated with WNK463 *ex vivo* producing significant amounts of these pro-inflammatory cytokines (**Extended Data Fig. 7a**).

RNAseq of efferocytic *Slc12a2*-deficient phagocytes showed a robust change in gene programs associated with oxidative stress (**Fig. 4b**). Oxidative stress, induced by accumulation of reactive oxygen species (ROS), is known to induce pro-inflammatory cytokine production,

including IL-1β[55]. Consistent with our RNAseq data, inhibition of the chloride-sensing pathway resulted in increased accumulation of ROS in efferocytic phagocytes *in vitro* (**Fig. 7c and Extended Data Fig. 7b**). Thymic macrophages treated with WNK463 during dexamethasone-induced apoptotic thymocyte clearance also showed significantly higher accumulation of ROS than vehicle treated controls (**Figure 7d**). Thus, the chloride-sensing pathway in phagocytes involving WNK and SLC12A2 is an important part of ROS regulation and normal suppression of the inflammatory response during efferocytosis *in vivo*.

Lastly, we asked whether forcing entry of extracellular chloride can reverse the pro-inflammatory responses. We allowed control or *Slc12a2*-deficient phagocytes to engulf apoptotic cells normally for 1 hour (by which time significant number of phagocytes have already engulfed but not digested corpses) and added the chloride ionophore TBTC. Treatment with TBTC significantly suppressed many of the pro-inflammatory genes in *Slc12a2*-deficient phagocytes, with the others (*Myd88*, *Nfkb2*, and *Tlr4*) being modestly decreased (**Fig. 7e**). Thus, forced chloride influx was sufficient to suppress the pro-inflammatory gene signature induced by *Slc12a2* deficiency during efferocytosis.

The data presented in this manuscript have several implications for efferocytosis in general and specifically for understanding how phagocytes interpret ingested apoptotic corpses as anti-inflammatory. First, this work identifies a previously unknown regulatory step that is induced within phagocytes after a corpse is internalized that involves SLC12A2 and kinases in the chloride-sensing pathway. Second, this chloride-sensing pathway controls cytosolic chloride flux during efferocytosis. Third, chloride flux during efferocytosis impacts the appetite of a given phagocyte, acting as a natural brake in efferocytosis. Fourth, when a phagocyte has disruption in the function of SLC12A2 or the upstream kinases, phagocytes fail to properly induce an anti-inflammatory gene program, a hallmark of efferocytosis. Further, *Slc12a2*-deficient phagocytes actively switch from a homeostatic efferocytosis signature to a pro-inflammatory program; this is not simply due to corpse overload as phagocytes engulfing multiple corpses in response to PtdSer receptor overexpression do not show a similar pro-inflammatory signature. A concept that has emerged from these studies is that the SLC12A2 pathway and chloride flux represent a ‘reversible switch’ controlling the anti- vs. pro-inflammatory response of a phagocyte after apoptotic cell uptake and could potentially be targeted for both dampening and promoting an immune response. Interestingly,

monogenic human diseases, such as Bartter's Syndrome or Gitelman's Syndrome, are caused by mutations in the SLC12 family of proteins as well as their regulators. The primary symptoms manifested in this constellation of syndromes are typically treatable; however, several case reports have suggested inflammatory disease sequelae that arise at later stages[56-59]. Whether routine efferocytosis is differentially 'interpreted' due to mutations in SLC12 pathway members is a possibility worthy of further exploration. In a recent study, treatment of RAW 264.7 macrophages with LPS resulted in increased uptake of fluorescent E. coli bioparticles, as well as increased proinflammatory cytokine release and this was attenuated via bumetanide pre-treatment[60]. This earlier work focused on SLC12A2 function in bacterial clearance/LPS responses (not efferocytosis); nevertheless, future studies are required to determine how the SLC12 pathway functions in different forms of phagocytosis and the associated immune responses, including bacterial, antibody-mediated, and complement-mediated clearance.

Acknowledgments

The authors thank members of the Ravichandran laboratory for discussions and critical reading of this manuscript; J.S.A.P. was supported by Cancer Research Institute – Mark Foundation Fellowship, NCI 1K99CA237728-01, Burroughs Wellcome PDEP award, and NCI Cancer Research Training Award 5T32CA009109-39. S.M. is supported by grants from the *Mishima-Kaiun* Memorial Foundation and The *Kanae Foundation* for the Promotion of Medical Science. This work was supported by grants to K.S.R. from the NIGMS (GM064709), NIMH (MH096484), NHLBI (P01HL120840), and the Center for Cell Clearance at the University of Virginia, Pilot funding from the UVa Brain Institute, Odysseus I award from the FWO, and an EOS grant from the FWO. E.D. is funded by NIH grants R21GM118944 and R01DK093501. C.M. is supported by the Pannexin Program Award through NHLBI (P01HL120840). M.H.R. was supported by the UVA Neuroscience Training Program 4T32GM008328-25. J.I.E. is supported by NIAID Training Award 5T32AI007496. C.D.L. is supported by an award from The Wellcome Trust (206566/Z/17/Z).

References

1. Arandjelovic, S. & Ravichandran, K.S. Phagocytosis of apoptotic cells in homeostasis. *Nat Immunol* **16**, 907-917 (2015).
2. Henson, P.M. Cell Removal: Efferocytosis. *Annual Review of Cell and Developmental Biology* **33**, 127-144 (2017).
3. Gordon, S. Phagocytosis: An Immunobiologic Process. *Immunity* **44**, 463-475 (2016).
4. Blander, J.M. The many ways tissue phagocytes respond to dying cells. *Immunological Reviews* **277**, 158-173 (2017).
5. Penberthy, K.K. & Ravichandran, K.S. Apoptotic cell recognition receptors and scavenger receptors. *Immunological Reviews* **269**, 44-59 (2016).
6. Elliott, M.R., Koster, K.M. & Murphy, P.S. Efferocytosis Signaling in the Regulation of Macrophage Inflammatory Responses. *The Journal of Immunology* **198**, 1387-1394 (2017).
7. Green, D.R., Oguin, T.H. & Martinez, J. The clearance of dying cells: table for two. *Cell Death And Differentiation* **23**, 915 (2016).
8. Davies, L.C., Jenkins, S.J., Allen, J.E. & Taylor, P.R. Tissue-resident macrophages. *Nature Immunology* **14**, 986 (2013).
9. Canton, J., Neculai, D. & Grinstein, S. Scavenger receptors in homeostasis and immunity. *Nature Reviews Immunology* **13**, 621 (2013).
10. Elliott, Michael R. & Ravichandran, Kodi S. The Dynamics of Apoptotic Cell Clearance. *Developmental Cell* **38**, 147-160 (2016).
11. Hochreiter-Hufford, A. & Ravichandran, K.S. Clearing the Dead: Apoptotic Cell Sensing, Recognition, Engulfment, and Digestion. *Cold Spring Harbor Perspectives in Biology* **5** (2013).
12. Segawa, K. & Nagata, S. An Apoptotic 'Eat Me' Signal: Phosphatidylserine Exposure. *Trends in Cell Biology* **25**, 639-650 (2015).
13. Levin, R., Grinstein, S. & Canton, J. The life cycle of phagosomes: formation, maturation, and resolution. *Immunological Reviews* **273**, 156-179 (2016).
14. Medina, C.B. & Ravichandran, K.S. Do not let death do us part: 'find-me' signals in communication between dying cells and the phagocytes. *Cell Death And Differentiation* **23**, 979 (2016).
15. Morioka, S. *et al*. Efferocytosis induces a novel SLC program to promote glucose uptake and lactate release. *Nature* (2018).
16. Bosurgi, L. *et al*. Macrophage function in tissue repair and remodeling requires IL-4 or IL-13 with apoptotic cells. **356**, 1072-1076 (2017).
17. Morioka, S., Maueröder, C. & Ravichandran, K.S. Living on the Edge: Efferocytosis at the Interface of Homeostasis and Pathology. *Immunity* **50**, 1149-1162 (2019).
18. Luo, B. *et al*. Erythropoeitin Signaling in Macrophages Promotes Dying Cell Clearance and Immune Tolerance. *Immunity* **44**, 287-302 (2016).
19. Kim, S., Elkon, K.B. & Ma, X. Transcriptional Suppression of Interleukin-12 Gene Expression following Phagocytosis of Apoptotic Cells. *Immunity* **21**, 643-653 (2004).
20. Chung, E.Y. *et al*. Interleukin-10 Expression in Macrophages during Phagocytosis of Apoptotic Cells Is Mediated by Homeodomain Proteins Pbx1 and Prep-1. *Immunity* **27**, 952-964 (2007).

21. Lucas, M. *et al*. Requirements for Apoptotic Cell Contact in Regulation of Macrophage Responses. *The Journal of Immunology* **177**, 4047-4054 (2006).
22. Fond, A.M., Lee, C.S., Schulman, I.G., Kiss, R.S. & Ravichandran, K.S. Apoptotic cells trigger a membrane-initiated pathway to increase ABCA1. *The Journal of Clinical Investigation* **125**, 2748-2758 (2015).
23. Alvey, C.M. *et al*. SIRPA-Inhibited, Marrow-Derived Macrophages Engorge, Accumulate, and Differentiate in Antibody-Targeted Regression of Solid Tumors. *Current Biology* **27**, 2065-2077.e2066 (2017).
24. Shekarabi, M. *et al*. WNK Kinase Signaling in Ion Homeostasis and Human Disease. *Cell Metabolism* **25**, 285-299 (2017).
25. Wang, G.G. *et al*. Quantitative production of macrophages or neutrophils ex vivo using conditional Hoxb8. *Nature Methods* **3**, 287 (2006).
26. Orlov, S.N., Koltsova, S.V., Kapilevich, L.V., Gusakova, S.V. & Dulin, N.O. NKCC1 and NKCC2: The pathogenetic role of cation-chloride cotransporters in hypertension. *Genes & Diseases* **2**, 186-196 (2015).
27. Delpire, E. & Gagnon, Kenneth B.E. SPAK and OSR1: STE20 kinases involved in the regulation of ion homoeostasis and volume control in mammalian cells. *Biochemical Journal* **409**, 321-331 (2008).
28. Flores, B., Schornak, C., Wolfe, L., Adams, D. & Delpire, E. Functional Characterization of the First Known Mutation of the Human SLC12A2 (NKCC1) Gene. *The FASEB Journal* **30**, 1224.1222 (2016).
29. Delpire, E. *et al*. A patient with multisystem dysfunction carries a truncation mutation in human SLC12A2, the gene encoding the Na-K-2Cl cotransporter, NKCC1. *Molecular Case Studies* **2** (2016).
30. Koumangoye, R., Omer, S. & Delpire, E. Mistargeting of a truncated Na-K-2Cl cotransporter in epithelial cells. *American Journal of Physiology-Cell Physiology* **0**, null.
31. Kahle, K.T. *et al*. WNK Protein Kinases Modulate Cellular Cl– Flux by Altering the Phosphorylation State of the Na-K-Cl and K-Cl Cotransporters. *Physiology* **21**, 326-335 (2006).
32. Miyanishi, M. *et al*. Identification of Tim4 as a phosphatidylserine receptor. *Nature* **450**, 435 (2007).
33. Park, D., Hochreiter-Hufford, A. & Ravichandran, K.S. The Phosphatidylserine Receptor TIM-4 Does Not Mediate Direct Signaling. *Current Biology* **19**, 346-351 (2009).
34. Lee, J. *et al*. A scaffold for signaling of Tim-4-mediated efferocytosis is formed by fibronectin. *Cell Death & Differentiation* (2018).
35. Yanagihashi, Y., Segawa, K., Maeda, R., Nabeshima, Y.-i. & Nagata, S. Mouse macrophages show different requirements for phosphatidylserine receptor Tim4 in efferocytosis. **114**, 8800-8805 (2017).
36. Anselmo, A.N. *et al*. WNK1 and OSR1 regulate the Na+, K+, 2Cl– cotransporter in HeLa cells. *Proceedings of the National Academy of Sciences* **103**, 10883-10888 (2006).
37. Vitari, Alberto C., Deak, M., Morrice, Nick A. & Alessi, Dario R. The WNK1 and WNK4 protein kinases that are mutated in Gordon's hypertension syndrome phosphorylate and activate SPAK and OSR1 protein kinases. *Biochemical Journal* **391**, 17-24 (2005).
38. Moriguchi, T. *et al*. WNK1 Regulates Phosphorylation of Cation-Chloride-coupled Cotransporters via the STE20-related Kinases, SPAK and OSR1. *Journal of Biological Chemistry* **280**, 42685-42693 (2005).

39. Vitari, Alberto C. *et al*. Functional interactions of the SPAK/OSR1 kinases with their upstream activator WNK1 and downstream substrate NKCC1. *Biochemical Journal* **397**, 223-231 (2006).
40. Rinehart, J. *et al*. Sites of Regulated Phosphorylation that Control K-Cl Cotransporter Activity. *Cell* **138**, 525-536 (2009).
41. Zagórska, A. *et al*. Regulation of activity and localization of the WNK1 protein kinase by hyperosmotic stress. *The Journal of Cell Biology* **176**, 89-100 (2007).
42. Yamada, K. *et al*. Small-molecule WNK inhibition regulates cardiovascular and renal function. *Nature Chemical Biology* **12**, 896 (2016).
43. Arroyo, J.P., Kahle, K.T. & Gamba, G. The SLC12 family of electroneutral cation-coupled chloride cotransporters. *Molecular Aspects of Medicine* **34**, 288-298 (2013).
44. Busetto, S., Trevisan, E., Decleva, E., Dri, P. & Menegazzi, R. Chloride Movements in Human Neutrophils during Phagocytosis: Characterization and Relationship to Granule Release. *The Journal of Immunology* **179**, 4110-4124 (2007).
45. Wang, G. Chloride flux in phagocytes. *Immunological Reviews* **273**, 219-231 (2016).
46. Koncz, C. & Daugirdas, J.T. Use of MQAE for measurement of intracellular [Cl-] in cultured aortic smooth muscle cells. *American Journal of Physiology-Heart and Circulatory Physiology* **267**, H2114-H2123 (1994).
47. Verkman, A.S., Sellers, M.C., Chao, A.C., Leung, T. & Ketcham, R. Synthesis and characterization of improved chloride-sensitive fluorescent indicators for biological applications. *Analytical Biochemistry* **178**, 355-361 (1989).
48. Albert, M.L., Kim, J.-I. & Birge, R.B. α v β 5 integrin recruits the CrkII–Dock180–Rac1 complex for phagocytosis of apoptotic cells. *Nature Cell Biology* **2**, 899-905 (2000).
49. Reddien, P.W. & Horvitz, H.R. CED-2/CrkII and CED-10/Rac control phagocytosis and cell migration in Caenorhabditis elegans. *Nature Cell Biology* **2**, 131 (2000).
50. Leverrier, Y. & Ridley, A.J. Requirement for Rho GTPases and PI 3-kinases during apoptotic cell phagocytosis by macrophages. *Current Biology* **11**, 195-199 (2001).
51. Tosello-Trampont, A.-C., Brugnera, E. & Ravichandran, K.S. Evidence for a Conserved Role for CrkII and Rac in Engulfment of Apoptotic Cells. **276**, 13797-13802 (2001).
52. deBakker, C.D. *et al*. Phagocytosis of apoptotic cells is regulated by a UNC-73/TRIO-MIG-2/RhoG signaling module and armadillo repeats of CED-12/ELMO. *Curr Biol* **14**, 2208-2216 (2004).
53. Nakaya, M., Tanaka, M., Okabe, Y., Hanayama, R. & Nagata, S. Opposite Effects of Rho Family GTPases on Engulfment of Apoptotic Cells by Macrophages. **281**, 8836-8842 (2006).
54. Lucas, C.D. *et al*. Downregulation of Mcl-1 has anti-inflammatory pro-resolution effects and enhances bacterial clearance from the lung. *Mucosal Immunology* **7**, 857 (2013).
55. Cruz, C.M. *et al*. ATP Activates a Reactive Oxygen Species-dependent Oxidative Stress Response and Secretion of Proinflammatory Cytokines in Macrophages. **282**, 2871-2879 (2007).
56. Mishima, E. *et al*. Inherited, not acquired, Gitelman syndrome in a patient with Sjögren's syndrome: importance of genetic testing to distinguish the two forms. *CEN Case Rep* **6**, 180-184 (2017).
57. Gu, X., Su, Z., Chen, M., Xu, Y. & Wang, Y. Acquired Gitelman syndrome in a primary Sjögren syndrome patient with a SLC12A3 heterozygous mutation: A case report and literature review. **22**, 652-655 (2017).

58. Zhou, H. *et al*. Complicated Gitelman syndrome and autoimmune thyroid disease: a case report with a new homozygous mutation in the SLC12A3 gene and literature review. **18**, 82 (2018).
59. Kusuda, T. *et al*. Acquired Gitelman Syndrome in an Anti-SSA Antibody-positive Patient with a SLC12A3 Heterozygous Mutation. *Internal Medicine* **55**, 3201-3204 (2016).
60. Hung, C.-M., Peng, C.-K., Wu, C.-P. & Huang, K.-L. Bumetanide attenuates acute lung injury by suppressing macrophage activation. *Biochemical Pharmacology* **156**, 60-67 (2018).

Fig. 1: Identification of corpse internalization-dependent gene programs in efferocytic phagocytes.

(a) Schematic for identifying the gene programs induced *after* corpse internalization. LR73 cells (fibroblasts from *C. griseus*) as phagocytes were cultured with apoptotic human Jurkat T cells in the absence (control) or presence of Cytochalasin D, which inhibits the uptake, but still allows corpse binding and phagocyte response to soluble signals released by apoptotic cells. By comparative analysis of transcriptional changes with and without Cytochalasin D, we could distinguish changes in gene expression due to soluble factors derived from apoptotic cells and corpse-contact, versus those requiring corpse-internalization. RNAseq of phagocytes treated with Cytochalasin D alone were also used to normalize. Analysis of transcripts that were differentially regulated during efferocytosis revealed a significant number of genes that were corpse internalization-dependent, as well as those that did not require internalization (see methods).

(b) Pathway analysis reveals a distinguishable pattern of gene program changes after corpse internalization. Shown are bidirectional plots representing the number of genes associated with a specific function / pathway that were significantly differentially regulated in response to either 'soluble factors / corpse contact' versus 'corpse internalization'. The transcriptional program that falls under general 'cell volume/size' regulation (green highlight) was chosen for further analysis. See also **Supplementary Table 1**.

Fig. 2: The SLC12A2 transporter functions as a 'brake' on apoptotic cell uptake.

(a) *Slc12a2*-deficient phagocytes engulf more apoptotic cells. Control or *Slc12a2*-deficient GFP+ LR73 phagocytes were co-cultured with CypHer5E-labeled apoptotic Jurkat cells for 2h and 8h, and analyzed by flow cytometry. Data are presented as phagocytosis index. Data represent n=4 independent experiments, shown as mean ± SEM. T-test, ***$p < .001$.

(b) *Slc12a2*-deficient BMDMs engulf more apoptotic corpses. Immortalized Cas9-GFP ER-Hoxb8 macrophage progenitors bearing *Slc12a2* or scrambled control guide RNAs, then differentiated into mature BMDMs, and assessed for uptake with CypHer5E-labeled apoptotic Jurkat cells for 1 h. Data represent n=4 independent experiments. Shown as mean ± SEM. T-test, ***$p < .001$.

(c) Macrophages from *Slc12a2*^{mut} mice bearing a SLC12A2 loss-of-function mutation engulf more apoptotic corpses. BMDMs from *Slc12a2*^{mut} mice or littermate controls were co-cultured with CypHer5E-labeled apoptotic thymocytes for 1 h and analyzed for efferocytosis. Data represent n=4 independent experiments. Shown as mean ± SEM. T-test, ***$p < .001$.

(d) *In vitro* inhibition of SLC12A2 in BMDMs increases apoptotic corpse uptake. BMDMs pre-treated for 1 h with 10μM Bumetanide were incubated with CypHer5E^{+} apoptotic Jurkat cells for 1h in the presence of drug or vehicle. Data from n=2 independent experiments.

(e) *In vivo* inhibition of SLC12A2 in thymic macrophages increases apoptotic corpse uptake. (left) CD45.2 bone marrow was mixed with bone marrow from mice (CD45.1/2) expressing TdTomato and injected into CD45.1 congenic recipient mice. After 8 weeks, recipient mice were treated with dexamethasone along with vehicle or 10μM Bumetanide. After 6h, CD45.2^{+} thymic macrophages were analyzed for engulfment of TdTomato+ cells. Data represent n=3 independent experiments, shown as mean ± SEM. T-test, ***$p < .001$.

(f) *Slc12a2*-deficient phagocytes engulf more apoptotic corpses on a per cell basis. Two hundred individual *Slc12a2*-deficient LR73 cells that took up apoptotic cells (CypHer5E+) were analyzed per replicate using ImageStream flow cytometry. Individual CypHer5E+ puncta (white arrow) were tabulated for individual phagocytes and scored as having 1, 2, 3 or ≥4 CypHer5E+ events. Fraction of the total CypHer5E+ population with different events per cell is shown. N=2 independent experiments. scale bar = 20 μM.

Fig. 3: Increased engulfment in SLC12A2 deficient phagocytes is not due to failure to degrade apoptotic cells

(a) Corpse degradation is not affected by *Slc12a2* deficiency in non-professional phagocytes. LR73 phagocytes were co-cultured with TAMRA-SE-labeled apoptotic Jurkat cells for 2h, washed, and cultured for another 6h to monitor degradation of TAMRA signal. Data are from n=2 independent experiments and shown as mean ± SEM. T-test, ns = not significant.

(b, c) Rate of corpse degradation is not affected in *Slc12a2*-deficient BMDMs. BMDMs lacking Slc12a2 or expressing a mutant Slc12a2 were co-cultured with TAMRA-SE-labeled apoptotic Jurkat cells for 1h, washed, then cultured for an additional 12 h to monitor degradation of TAMRA signal. Data are from n=3 independent experiments. Data shown as mean ± SEM. T-test, ns = not significant.

(d, e) Efferocytic *Slc12a2*-deficient phagocytes do not have disrupted lysosomal acidification. LR73 cells or macrophages were labeled with the lysosomal pH indicator LysoSensor prior to co-culture with CypHer5E+ apoptotic cells and analyzed for LysoSensor MFI. Data are presented as the Geometric Mean Fluorescence Intensity (MFI). Flow cytometry plot (left) or summarized data from n=3 experiments (right) are shown as mean ± SEM. T-test, ns = not significant.

(f, g) *Slc12a2*-deficient phagocytes engulf significantly more corpses without an effect on lysosomal acidification. *Slc12a2*-deficient LR73 phagocytes or macrophages were mixed with CellTrace Far Red-labeled apoptotic Jurkat cells (2h or 1h, respectively) and the lysosomal acidification-inhibitor Bafilomycin A. Data from n=3 independent experiments are shown as mean ± SEM. T-test. $^{**}p < .01$.

(h, i) Phagolysosomal function is preserved in *Slc12a2*-deficient phagocytes. Control or *Slc12a2*-deficient LR73 cells or BMDMs were co-cultured with DQ-Red-BSA labeled apoptotic Jurkat cells for 2h and the fluorescence from DQ-Red that arises within phagolysosomes assessed. Data are from n=3 independent experiments and shown as mean ± SEM. T-test, $^{**}p < .01$.

Fig. 4. Loss of SLC12A2 disturbs the homeostatic efferocytosis-associated gene signature.

(a) Schematic of the RNAseq analysis of *Slc12a2*-deficient phagocytes engulfing apoptotic cells. *Slc12a2*-deficient or control LR73 phagocytes were cultured with CypHer5E-labeled apoptotic Jurkat cells for 2 h. Phagocytes were collected and CypHer5E+ cells (i.e. engulfing phagocytes) were sorted directly into lysis buffer for RNAseq analysis. Image representative of 4 experiments.

(b) *Slc12a2*-deficient phagocytes display altered homeostatic efferocytosis transcriptional signatures. RNAseq data from *Slc12a2*-deficient and control phagocytes was analyzed for expression of the corpse internalization-dependent transcriptional programs including the anti-inflammatory, pro-inflammatory, and oxidative stress programs identified in **Fig. 1**. Shown are heatmaps representing differentially expressed pro-inflammatory, anti-inflammatory, and oxidative stress genes in control vs *Slc12a2*-deficient efferocytic phagocytes. Data are from four independent experiments. See also **Extended Data Fig. 3** and **Supplementary Table 2**.

(c) Enhanced corpse uptake due to PtdSer receptor overexpression does not induce a pro-inflammatory gene signature. Control, *Slc12a2*-deficient, and Tim4 expressing LR73 cells were fed with Jurkat cells for 2 h. CypHer5E^{+} phagocytes were sorted, and the expression of selected pro-inflammatory genes was determined by qPCR. Data are from n=3 independent experiments. Data shown as mean ± SEM. T-test, ***$p < .001$. ns = not significant.

Fig. 5. SLC12 family-linked kinases also regulate efferocytosis.

(a) Model of the WNK1-OSR1/SPAK-SLC12A2/SLC12A4 pathway of electroneutral chloride sensing and chloride flux. WNK1 is inactive bound to chloride. Upon chloride efflux, WNK1 is activated and phosphorylates either OSR1 or SPAK (or both). OSR1 and SPAK then phosphorylate both SLC12A2 and SLC12A4, with phosphorylation opening SLC12A2 (allowing chloride influx) and closing SLC12A4 (blocking chloride efflux).

(b-d) Reduction in *Oxsr1* (OSR1), *Stk39* (SPAK), and *Wnk1* results in a similar increase in apoptotic cell clearance as *Slc12a2* deficiency. siRNA-mediated reduction of *Oxsr1* (OSR1, b), *Stk39* (SPAK, c), or *Wnk1* (d) in LR73 phagocytes display significantly increased apoptotic cell uptake. Phagocytosis index is relative to control phagocytes (2h). Data represent at least four independent experiments for 2 h and two independent experiments for 8 h time points.

(e) WNK1 deficiency phenocopies *Slc12a2* deficiency in phagocytes during efferocytosis. LR73 phagocytes lacking WNK1 (via CRISPR/Cas9-mediated deletion) were co-cultured with CypHer5E-labeled apoptotic Jurkat cells for 2 h and 8 h. Phagocytosis index relative to control shown from n=4 independent experiments. One-Way ANOVA, ***$p < .001$.

(f, g) Inhibition of WNK leads to efferocytosis increase by BMDMs and peritoneal macrophages *in vitro*. CFSE-labeled BMDMs or peritoneal macrophages were pre-treated with vehicle or WNK463 for 1h prior to and during efferocytosis with CypHer5E+ apoptotic Jurkat cells. Phagocytosis index relative to vehicle-treated phagocytes is shown from at least n=3 independent experiments as (f) mean ± SEM. (g) mean ± SD, T-test, ***$p < .001$.

(h) *In vivo* inhibition of WNK in thymic macrophages increases apoptotic corpse uptake. (left) Similar to **Fig. 2e**. (right) Thymic macrophages were analyzed for engulfment of TdTomato+ cells. Data from three independent experiments (n=5 mice per condition) shown as mean ± SEM. T-test, ***$p < .001$.

(i) WNK inhibitor enhances efferocytosis by peritoneal macrophages *in vivo*. Mice were injected (i.p) with WNK463 for 30 min prior to co-injection of CypHer5E-labeled apoptotic Jurkat cells (with WNK463 inhibitor). After 30 min, CD11b+ F4/80+ macrophages were analyzed for apoptotic cell uptake. Data are from three independent experiments (Vehicle n=5, WNK463 n=6), shown as mean ± SEM. T-test, **$p < .01$.

Fig. 6. Chloride flux during efferocytosis.

(a) Elevated intracellular chloride level impairs efferocytosis and suppresses increased engulfment in *Slc12a2*-deficient phagocytes. Control or *Slc12a2*-deficient LR73 phagocytes were co-cultured with CypHer5E-labeled apoptotic Jurkat cells for 2h with or without TBTC, and efferocytosis assessed. Data represent n=2 independent experiments.

(b, c) MQAE-mediated monitoring of intracellular chloride during efferocytosis. LR73 phagocytes were labeled with MQAE (b), and co-cultured with or without CypHer5E+ apoptotic thymocytes for 2h (shown) or 6h (**Extended Data Fig. 6b**). Gated efferocytic phagocytes (CypHer5E high) show proportionally lower chloride levels, i.e. MQAE "bright" (c). Plots represent three independent experiments.

(d, e) Disruption of *Slc12a2* or *Slc12a4* affects chloride flux during efferocytosis. *Slc12a2* and *Slc12a4* were targeted via siRNA, and MQAE-labeled LR73 cells were co-cultured with CypHer5E-labeled apoptotic thymocytes for 2h. Representative plots (d), and compiled data from independent experiments (e) of CypHer5E+ MQAE "bright" (see also **Extended Data Fig. 6c**) phagocytes are shown. Data from n=3 independent experiments (bar = mean). One-way ANOVA, ***$p < .001$.

(f) Increased corpse binding in *Slc12a2*-deficient phagocytes can be rescued using the chloride ionophore TBTC. *Slc12a2*-deficient or control GFP+ LR73 phagocytes were pre-treated with or without TBTC (6h) and Cytochalasin D (1h), then co-cultured with TAMRA-SE-labeled apoptotic cells and assessed for binding via flow cytometry. Frequency of bound corpses (left) and corpse-derived fluorescence (MFI, right panel) were assessed. Data represent n=3 independent experiments (bar = mean ± SD). Two-way ANOVA, ** $p < .01$, *** $p < .001$.

(g) *Slc12a2*-deficient phagocytes exhibit a robust integrin pathway associated signature. Heatmap of genes coding for integrin and downstream signaling molecules (red) in efferocytic *Slc12a2*-deficient phagocytes compared to control phagocytes (from RNAseq data of **Fig. 4a**).

(h) *Slc12a2*-deficient phagocytes exhibit increased phosphatidylserine- and integrin-dependent binding of apoptotic cells. Similar to (f), except ACs were pre-treated with Annexin V or phagocytes pre-treated with RGDS peptide for 30 min. Data represent n=3 independent experiments (bar = mean ± SD). Two-way ANOVA, * $p < .05$, ** $p < .01$, *** $p < .001$.

Fig. 7. The SLC12 pathway and chloride flux are required to prevent inflammatory apoptotic cell clearance.

(a, b) *In vivo* inhibition of SLC12A2 or WNK family members impairs inflammation resolution. (a) Schematic of *in vivo* LPS-inflammation model in the lung (top) and analysis of pro-inflammatory and anti-inflammatory cytokines in bronchoalveolar lavage fluid (cell-free) assessed via Luminex assay (bottom). (b) Isolated alveolar macrophages were assessed for pro-inflammatory genes via qPCR. n.d. = not detected, Data from vehicle (n=10 except n=5 for IL-10), bumetanide (n=5 except n=9 for IL-1b), and WNK463 (n=9, except n=5 for IL-10) biological replicates, shown as mean ± SEM. One-way ANOVA, $*p < .05$, $**p < .01$, $***p < .001$.

(c) The SLC12 pathway affects ROS levels in non-professional phagocytes *in vitro*. LR73 phagocytes were labeled with oxidative stress indicator CellROX, which fluoresces in response to oxidation by ROS. Phagocytes were co-cultured with apoptotic cells, and levels of ROS assessed by flow cytometry. Data from n=4 independent experiments are shown as mean ± SEM. T-test, $***p < .001$.

(d) The SLC12 pathway regulates ROS levels by professional phagocytes *in vivo*. C57BL/6J mice were treated with dexamethasone (Dex) to induce thymocyte death and co-injected with either WNK463 or vehicle. Thymic macrophages were isolated after 6 hours, and analyzed for oxidative stress using CellROX readout via flow cytometry. Data are from two independent experiments (n=7 mice), and shown as mean ± SEM. T-test, $***p < .001$.

(e) Forced chloride influx suppresses pro-inflammatory gene signature. Control or *Slc12a2*-deficient phagocytes were co-cultured with apoptotic cells for a total of 2 h. At the 1h time point with apoptotic cells, the chloride ionophore TBTC was added to half of the wells in each condition. Phagocytes were harvested and assessed via qPCR for the presence of pro-inflammatory genes shown. Data are from n=2 independent experiments.

Fig. 1: Identification of corpse internalization-dependent signals in engulfing phagocytes

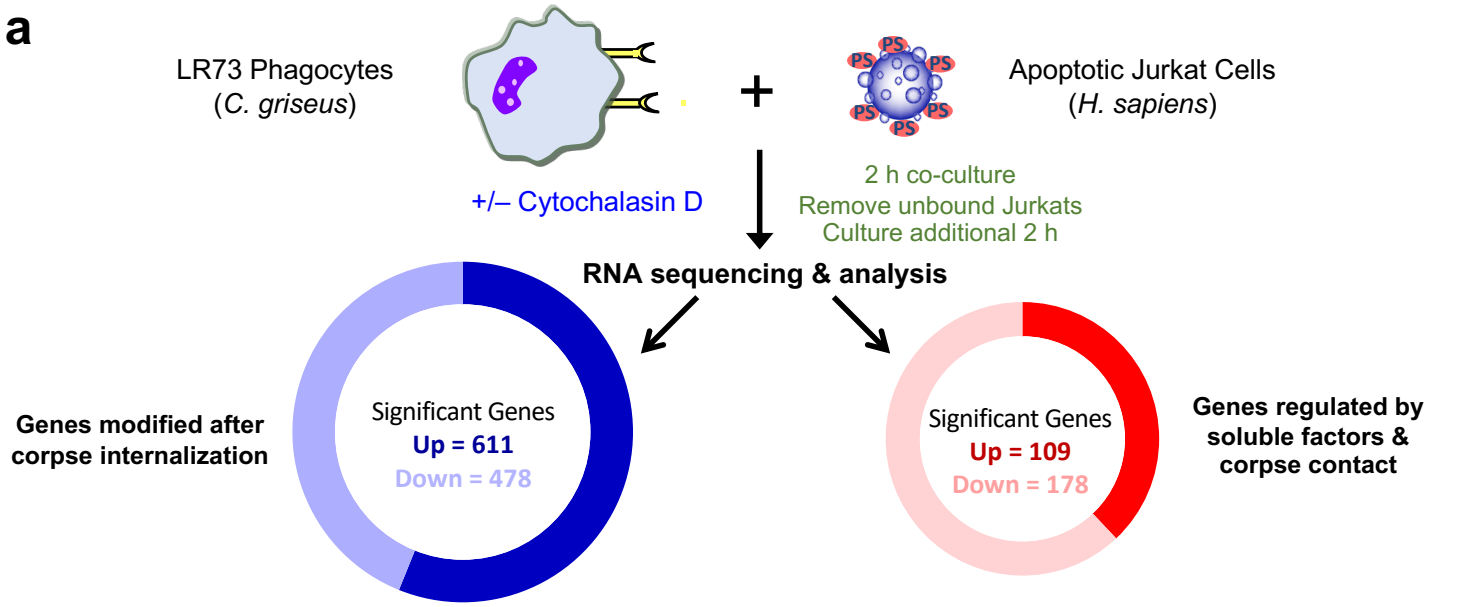

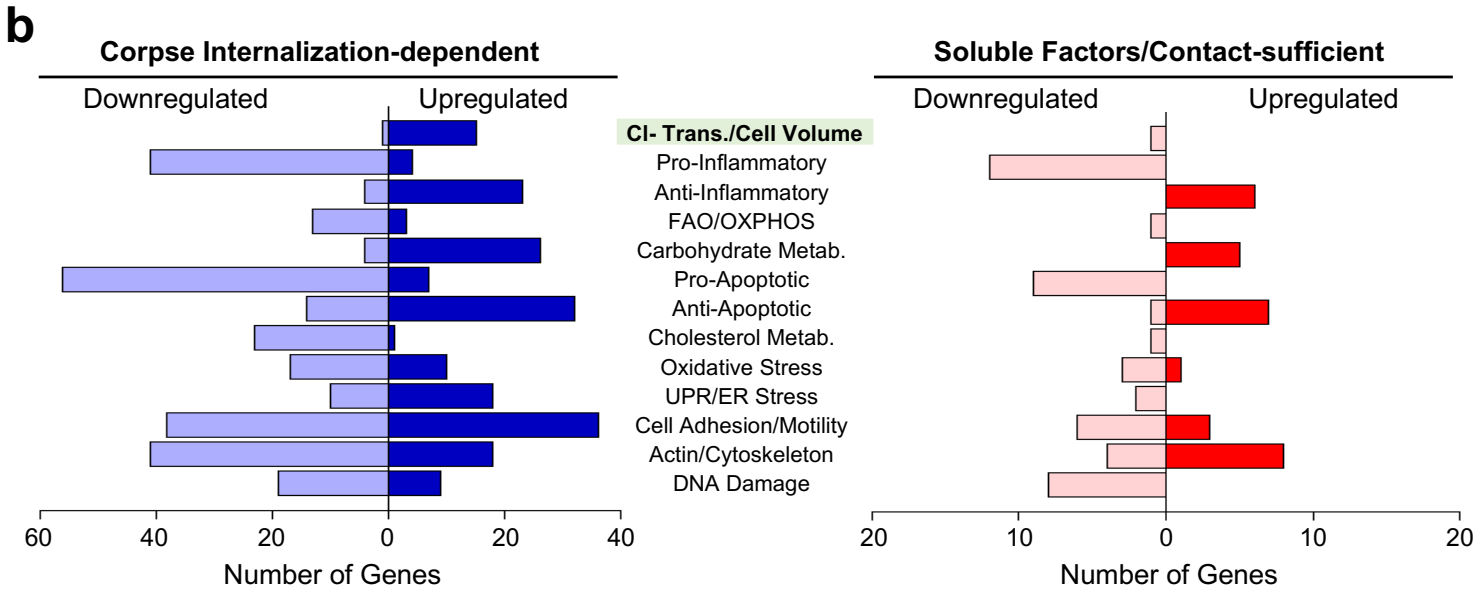

c

Cell volume/size-regulation associated genes

Gene	Protein Name	Protein Characteristic	Corpse Internalization Dependent	Soluble Factors/ Contact-Sufficient	Adjusted *p* value	Log_2 Fold Change
Slc12a2	SLC12A2, NKCC1	Electroneutral Na-K-Cl cotransporter	Upregulated	No Change	5.13E-03	0.623
Slc12a4	SLC12A4, KCC1	Electroneutral K-Cl cotransporter	Downregulated	No Change	1.52E-07	-0.312
Stk39	SPAK	STE20/SPS1-related proline-alanine-rich kinase	Upregulated	No Change	3.37E-02	0.134
Oxsr1	OSR1	Serine/threonine-protein kinase OSR1	Upregulated	No Change	5.20E-07	0.220

Fig. 2: SLC12A2 functions as a 'brake' on apoptotic cell uptake

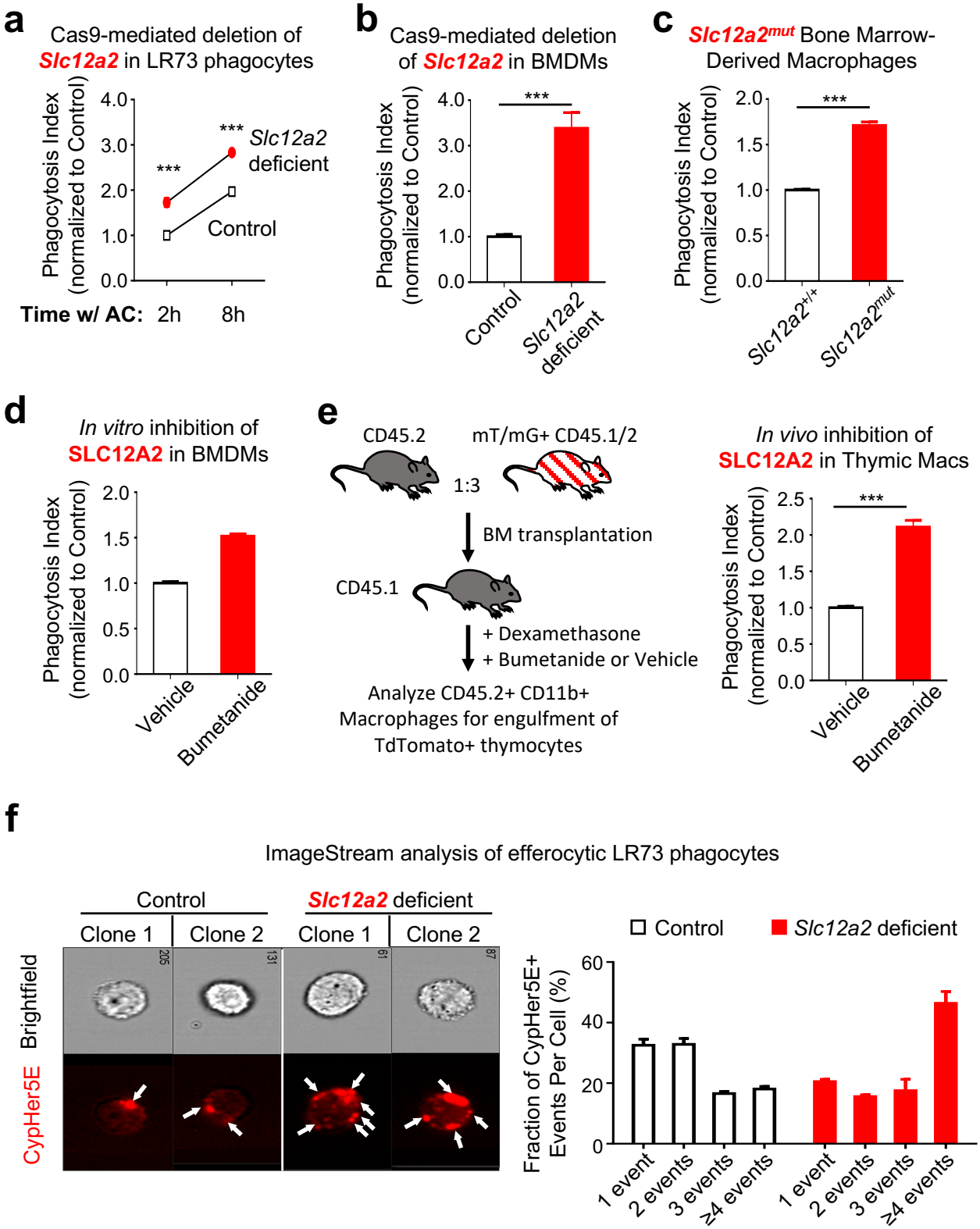

Fig. 3: Boosted engulfment in SLC12A2 deficient phagocytes is not due to failure to degrade apoptotic cells

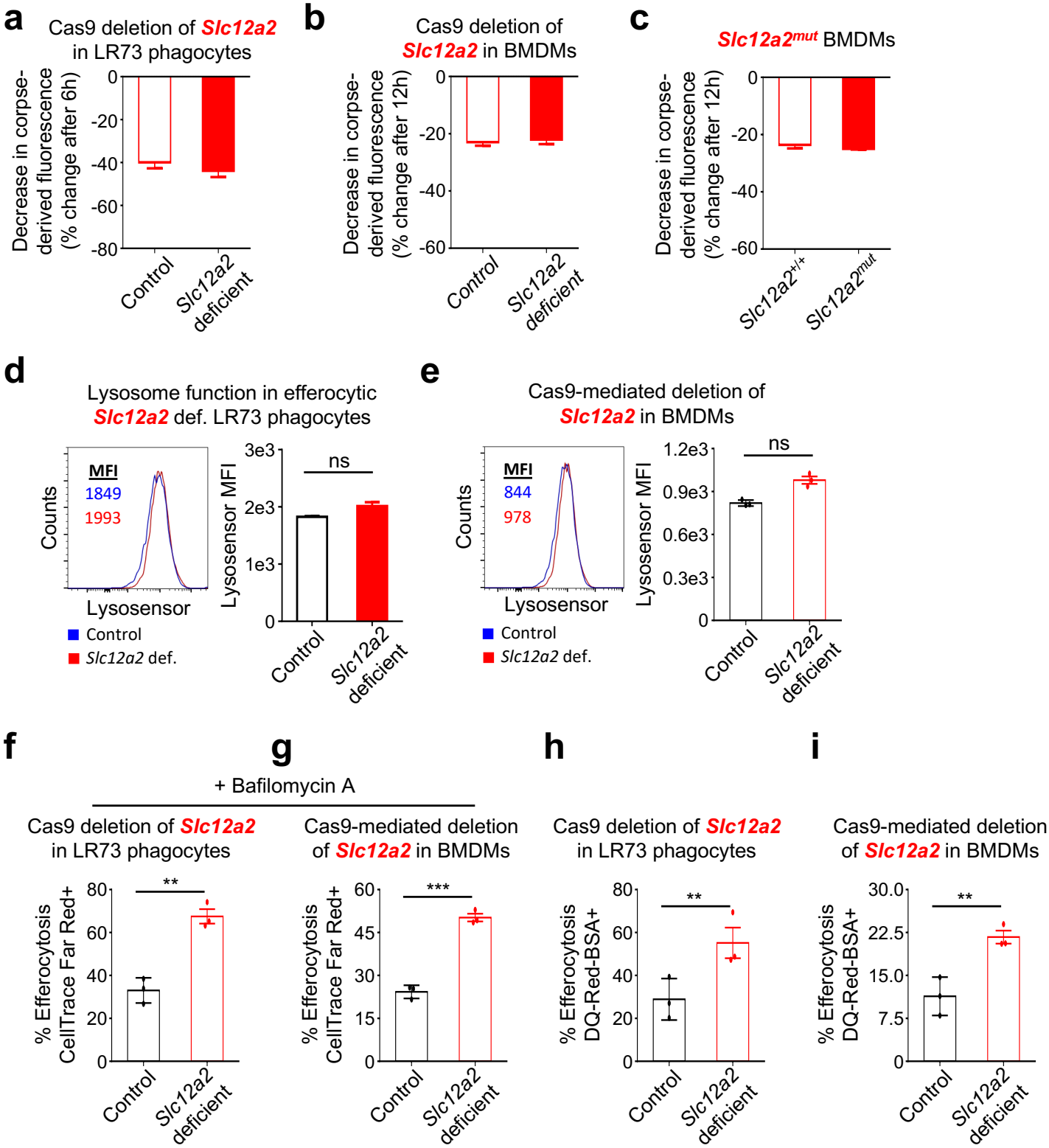

Fig. 4. SLC12A2 enforces a homeostatic efferocytosis signature

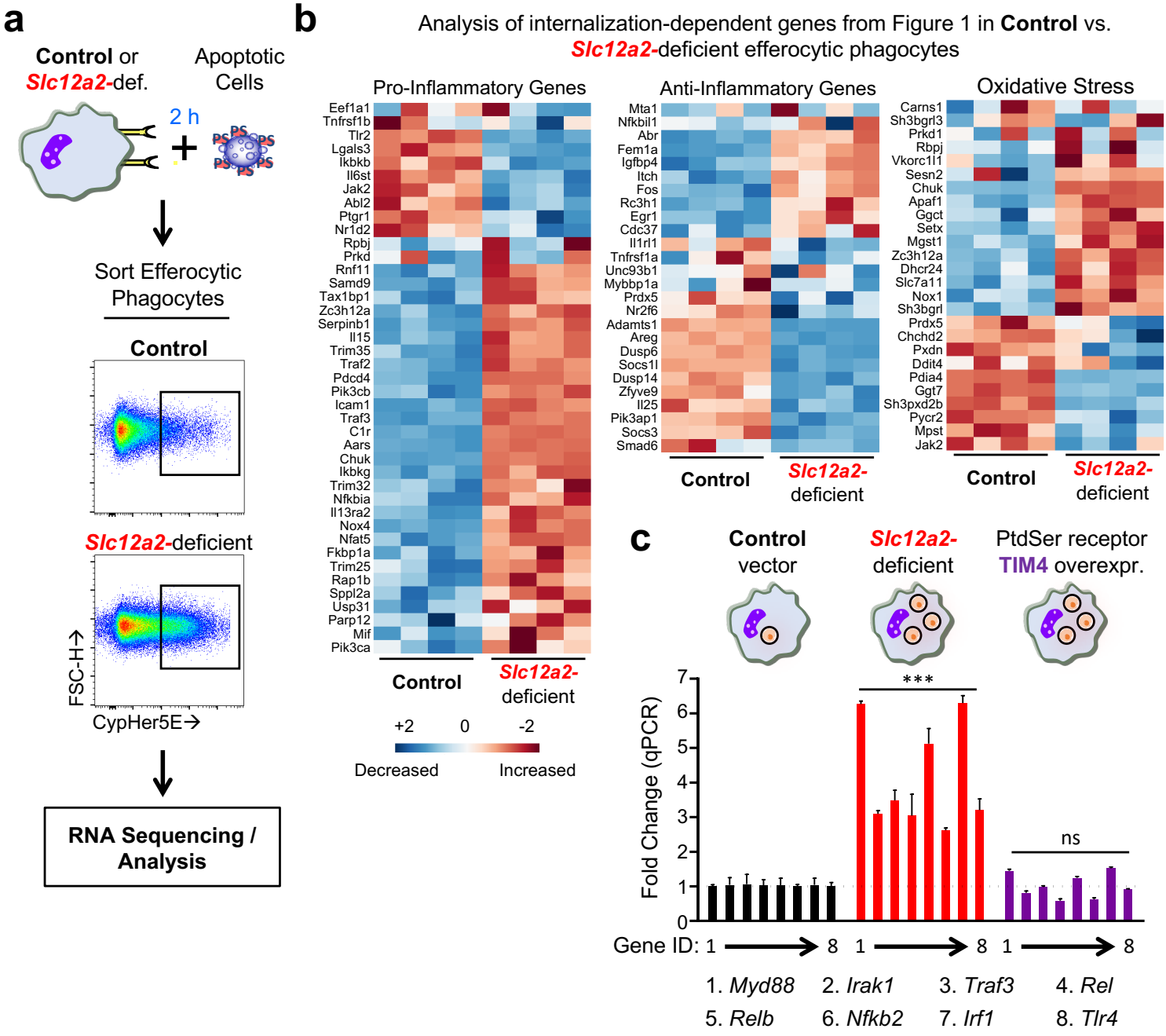

Fig. 5. SLC12 family-associated kinases also regulate rate of corpse uptake

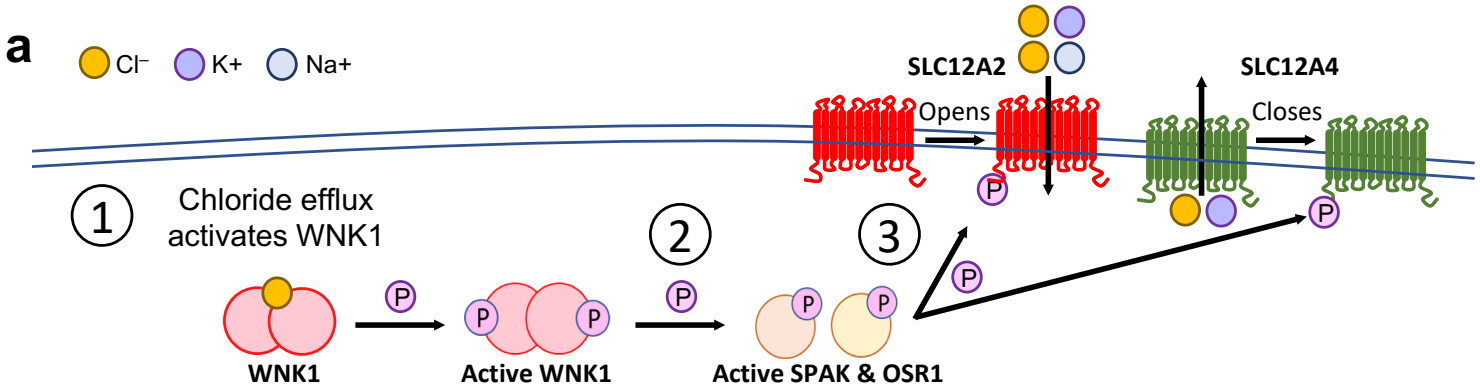

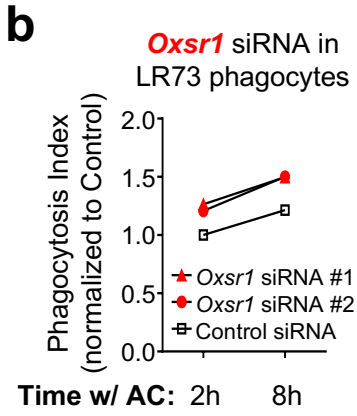

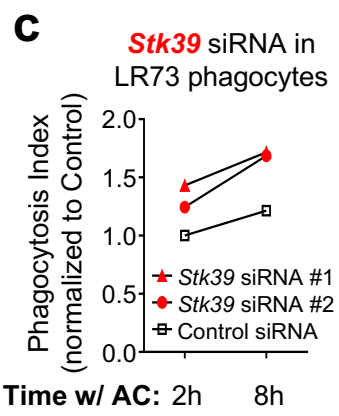

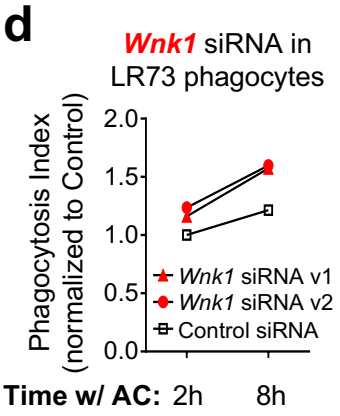

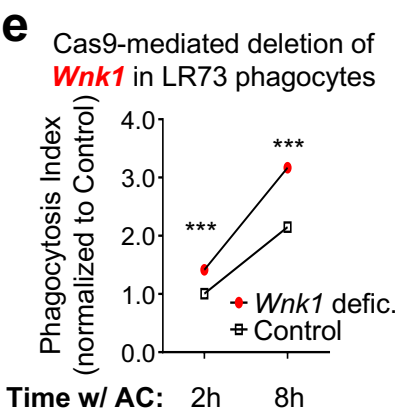

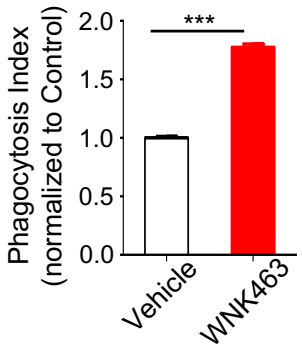

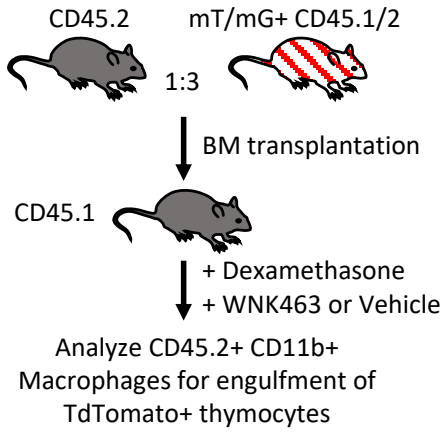

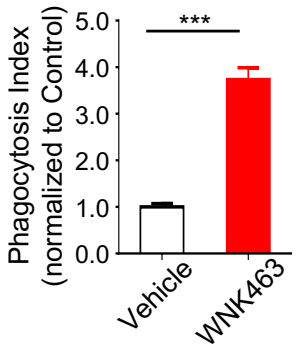

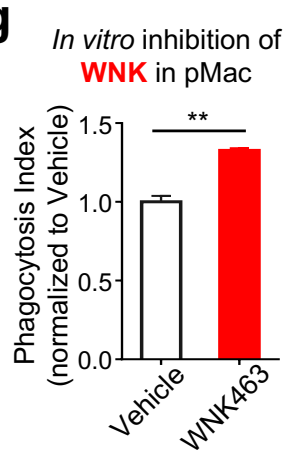

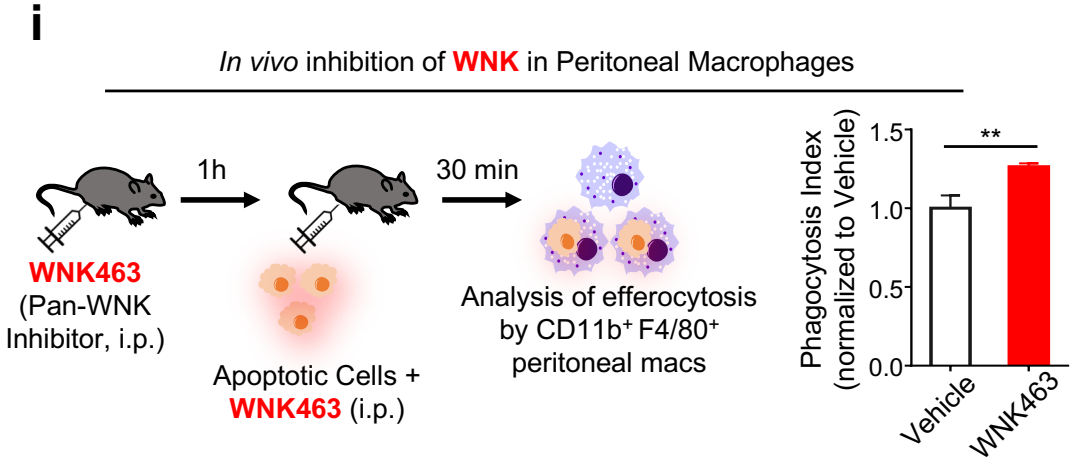

Fig. 6. Chloride efflux and influx act as "accelerator" and "brake" during efferocytosis

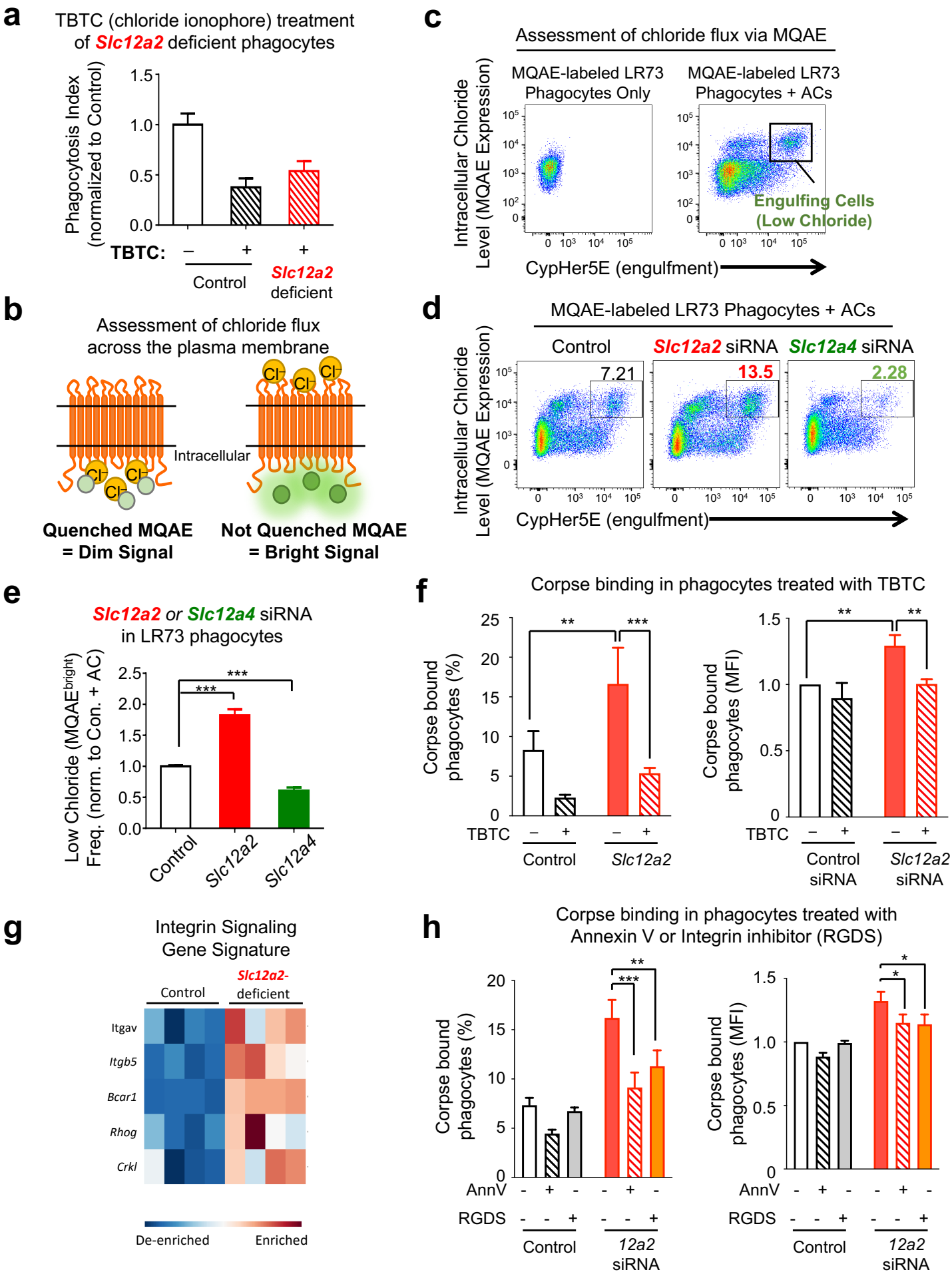

Fig. 7. The SLC12 pathway and chloride flux are required to prevent inflammatory apoptotic cell clearance

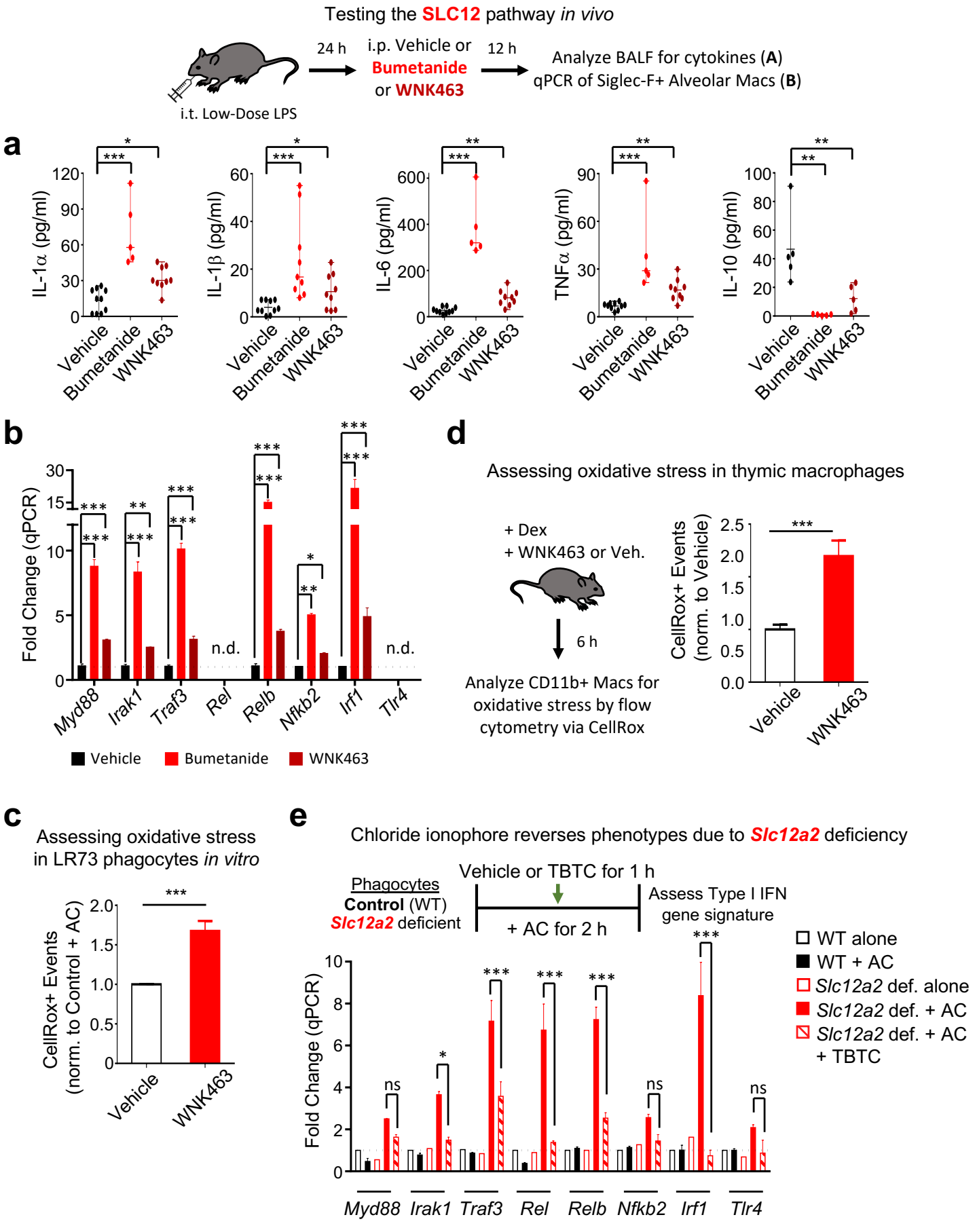

Supplementary Figures S1 through S7, Supplementary Videos 1-6, and Supplementary Table 1

(that relate to the Main Figures)

Justin S. A. Perry, Sho Morioka, et al.

Supplementary Figure S1. Related to Figure 1 & 2.

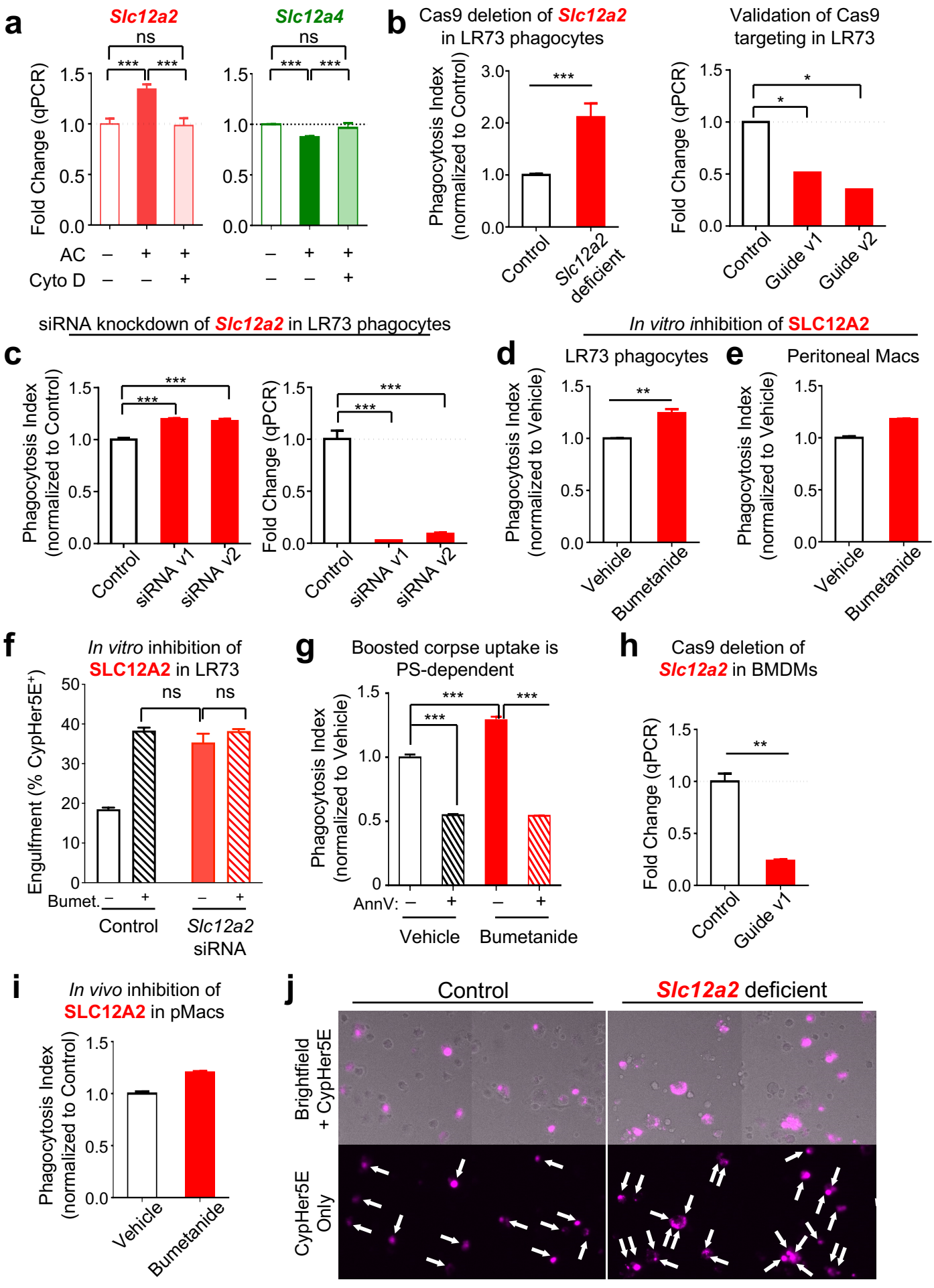

Supplementary Figure S2. Related to Figure 1 & 3

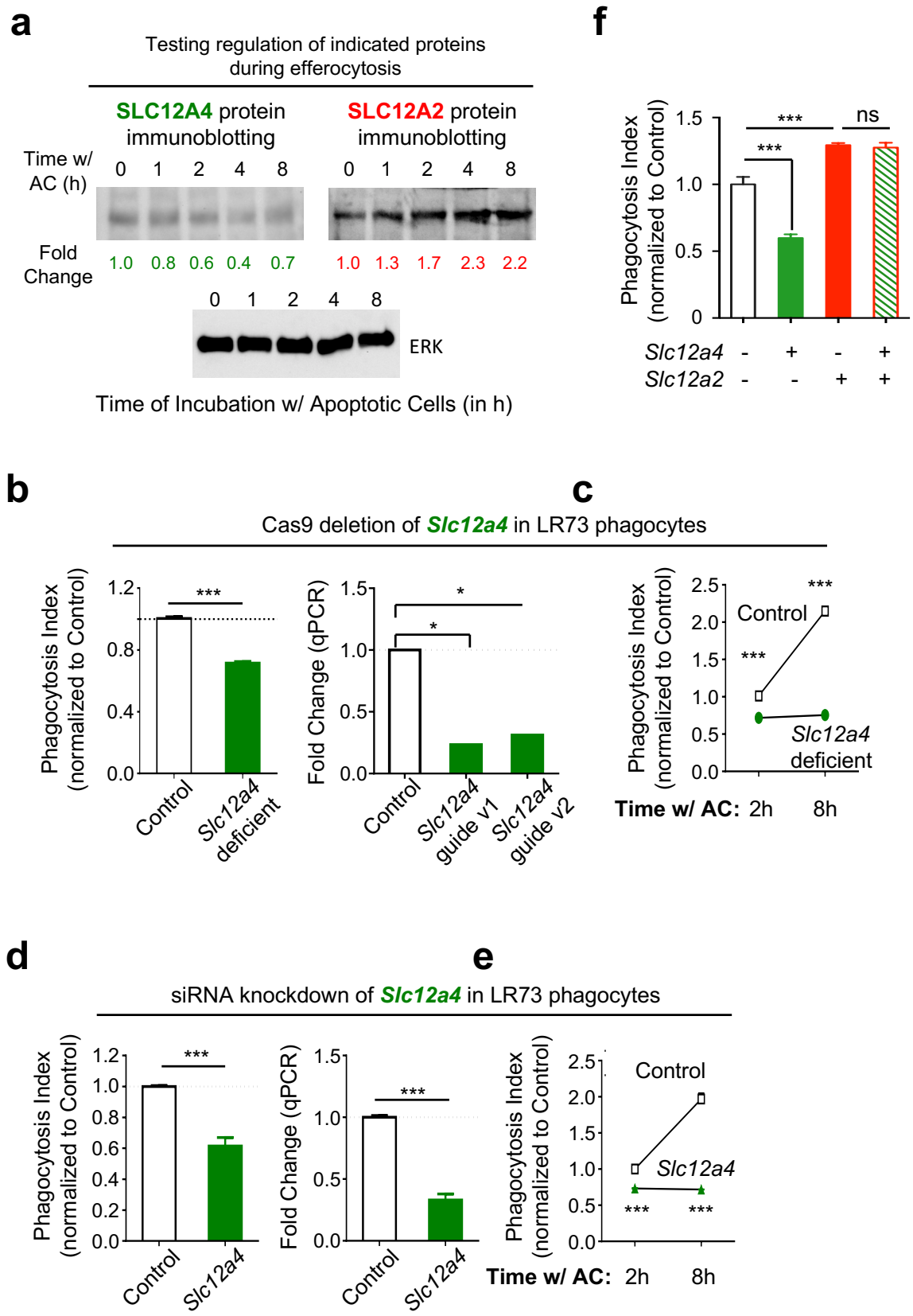

Supplementary Figure S3. Related to Figure 4.

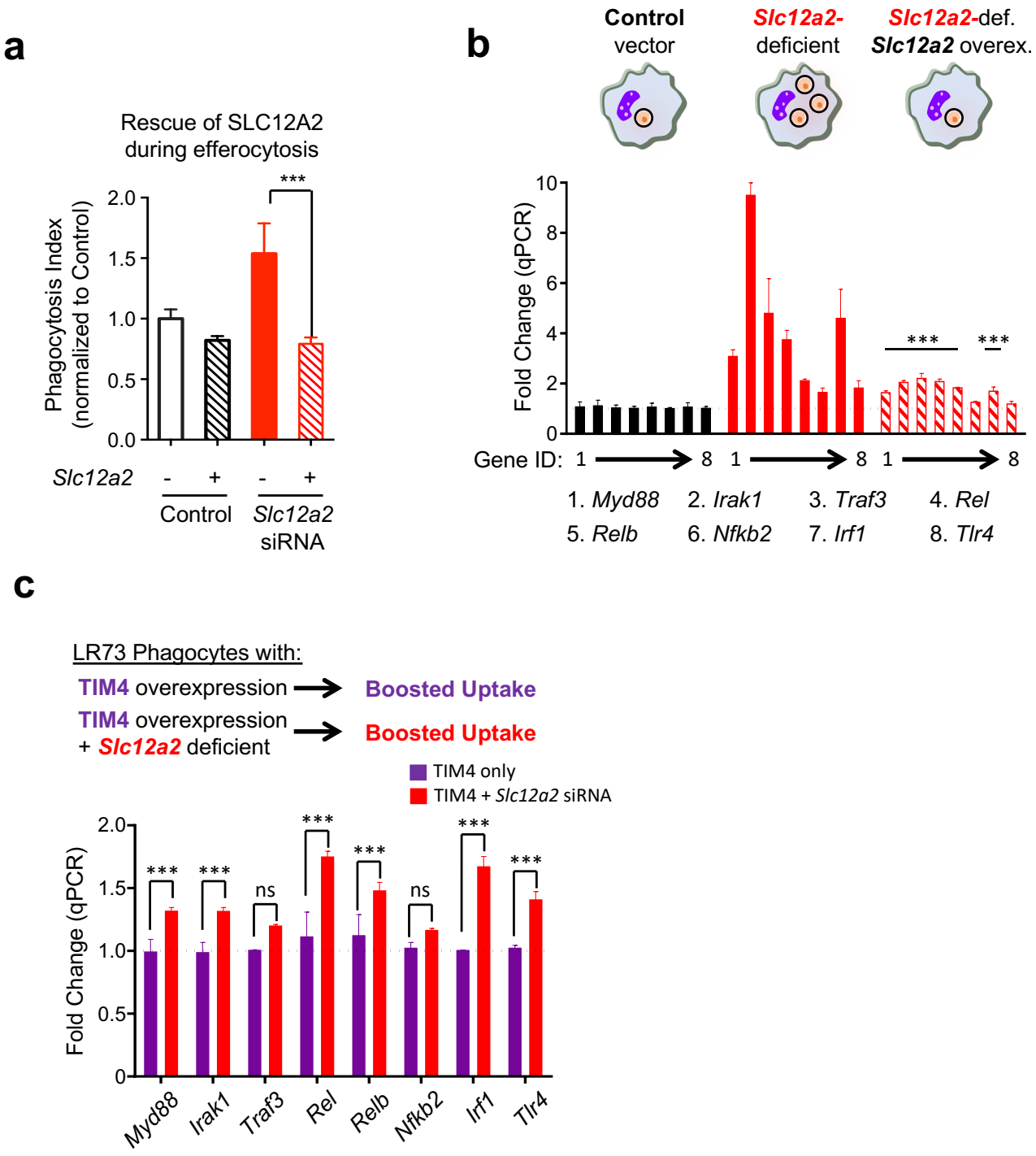

Supplementary Figure S4. Related to Figure 5.

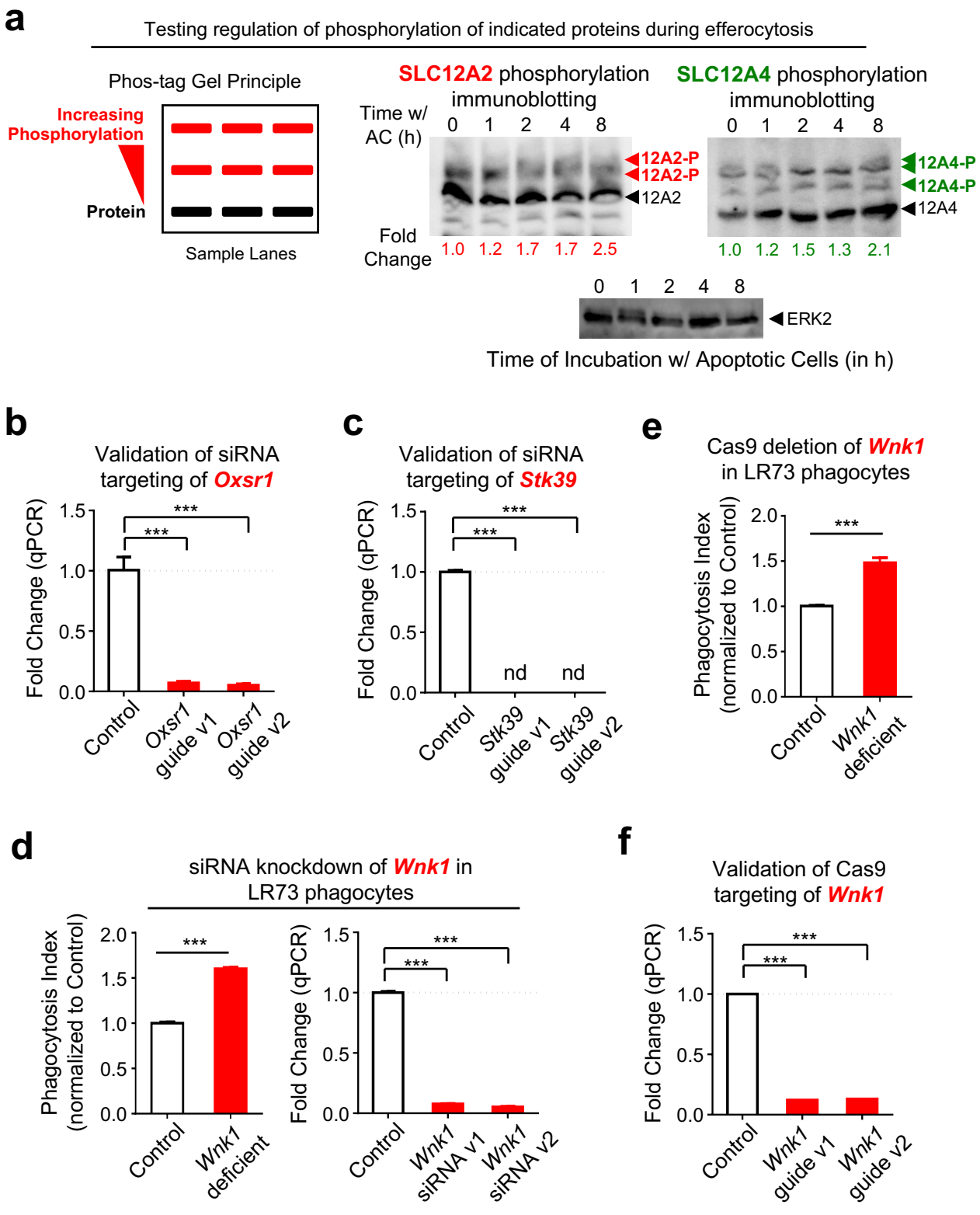

Supplementary Figure S5. Related to Figure 2 & 5.

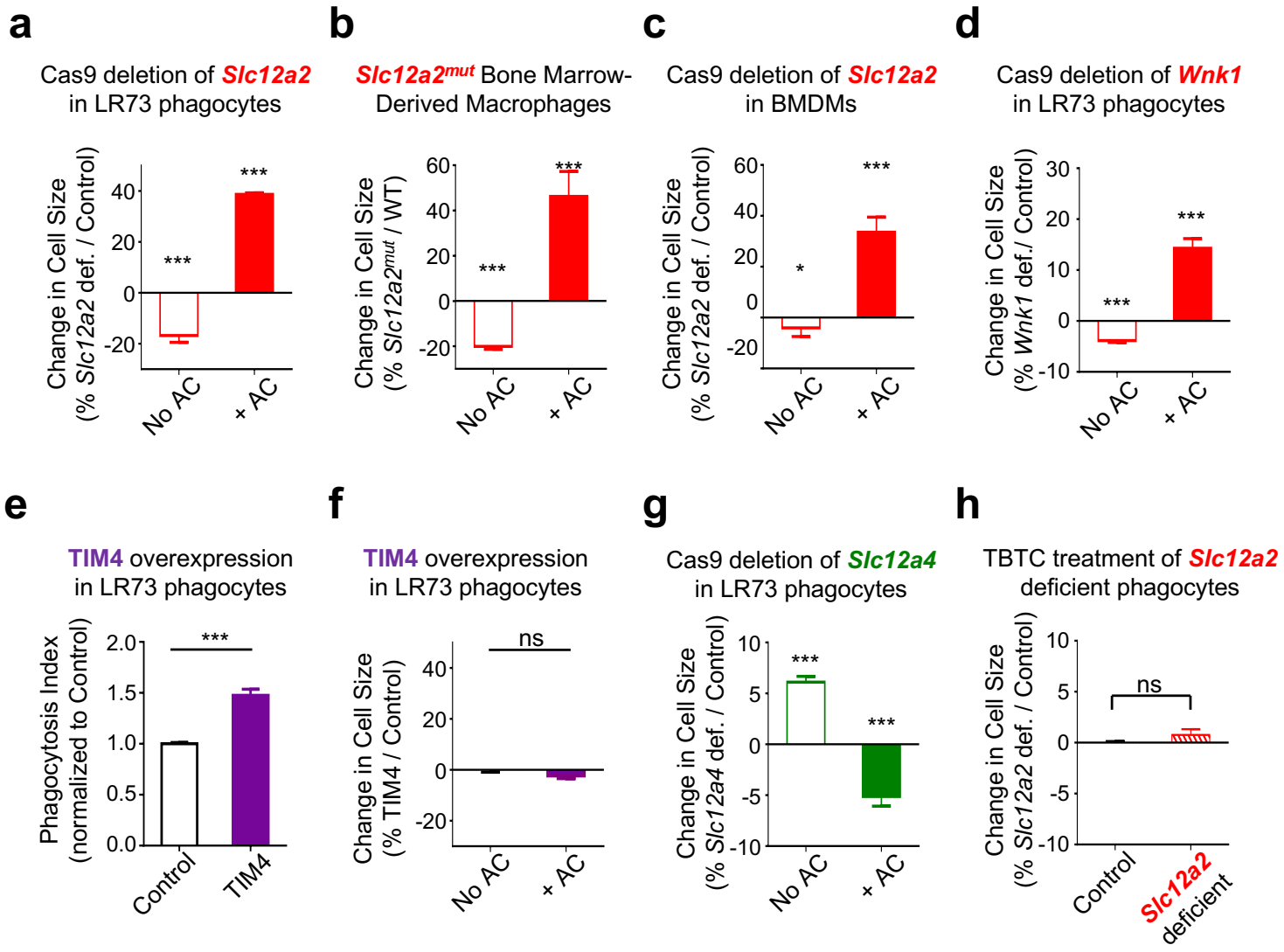

Supplementary Figure S6. Related to Figure 6.

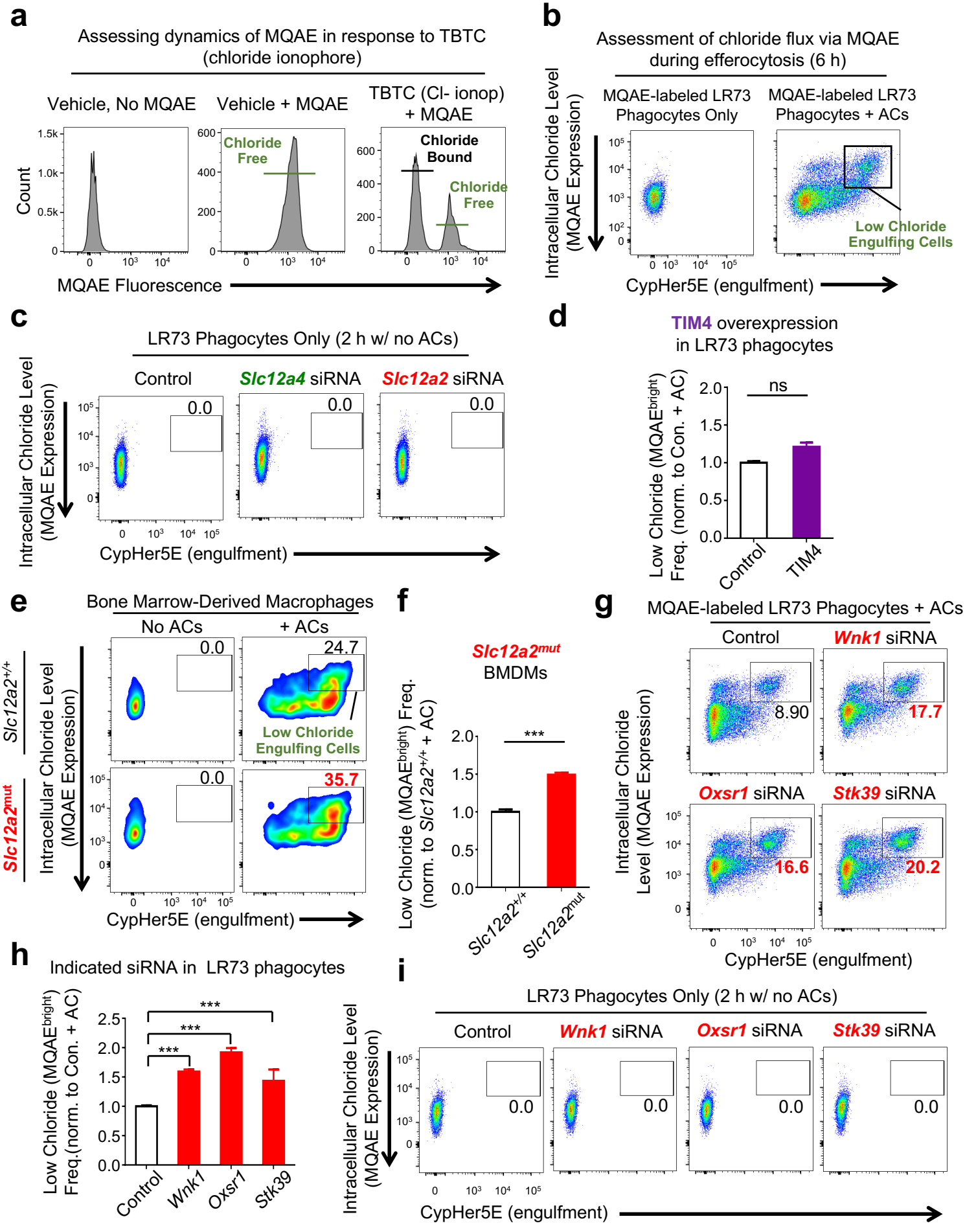

Supplementary Figure S7. Related to Figure 7.